



Cite this: *J. Mater. Chem. C*, 2016,  
4, 3041

## Tetraaryl pyrenes: photophysical properties, computational studies, crystal structures, and application in OLEDs†

Tarek H. El-Assaad,<sup>a</sup> Manuel Auer,<sup>b</sup> Raul Castañeda,<sup>c</sup> Kassem M. Hallal,<sup>a</sup> Fadi M. Jradi,<sup>a</sup> Lorenzo Mosca,<sup>d</sup> Rony S. Khnayzer,<sup>e</sup> Digambara Patra,<sup>a</sup> Tatiana V. Timofeeva,<sup>c</sup> Jean-Luc Brédas,<sup>f</sup> Emil J. W. List-Kratochvil,<sup>bg</sup> Brigitte Wex\*<sup>e</sup> and Bilal R. Kaafarani\*<sup>a</sup>

Pyrene was derivatized in positions 1, 3, 6, and 8 to yield a series of nine tetraarylpyrenes for which absorption, emission, emission lifetimes and solvatochromism in solution were determined. The fluorescence quantum yields in thin films and crystalline state, electrochemistry, and quantum-chemical calculations were completed for the series along with the X-ray crystal structure analysis of compounds **1**, **2**, **4**, **5**, **7**, and **9**. Compounds **2**, **3**, **4** as well as **7** were identified as the most suitable candidates for OLED application. Notably, in an unoptimized single-layer device geometry, these compounds exhibited blue electroluminescence coupled with impressively low turn-on voltages and high maximum luminances such as 2.8 V and 13 542 cd m<sup>-2</sup> at 8.2 V for compound **2**, respectively.

Received 10th September 2015,  
Accepted 1st October 2015

DOI: 10.1039/c5tc02849c

www.rsc.org/MaterialsC

### Introduction

Pyrene, a polycyclic aromatic hydrocarbon, has made a broad impact on a wide range of scientific fields such as analytical<sup>1,2</sup> and bioorganic chemistry<sup>3</sup> as well as organic electronics, as reported by Figueira-Duarte and Müllen<sup>4</sup> in their recent seminal review. Therein, the significance of the pyrene core, particularly as a material combining high chemical stability, charge-carrier mobility and blue-light emission was highlighted for use in organic light-emitting diodes (OLEDs).<sup>4</sup> The fluorescent nature of pyrene<sup>5-7</sup> and the pyrene excimer<sup>5,8-10</sup> has been widely

investigated both in the solid state and in solution. The pyrene excimer is an interaction between a ground state and an excited state molecule when in close proximity and is characterized by a marked bathochromic shift in the maximum emission wavelength.<sup>7</sup> To overcome excimer formation, steric functionalization of the pyrene core is necessary.<sup>11</sup> Synthetic strategies for substitution at various positions were thoroughly reviewed<sup>4,12</sup> and a wealth of pyrene derivatives have been studied for emissive properties and application in optoelectronic devices such as monosubstituted pyrenes,<sup>13,14</sup> 1,3-disubstituted pyrenes,<sup>15</sup> 1,6-disubstituted pyrenes,<sup>16</sup> 1,8-disubstituted pyrenes,<sup>17</sup> and 2,7-disubstituted pyrenes.<sup>18-20</sup> Y-shaped, 1,3,7-trisubstituted pyrene derivatives exhibit blue emission with medium to high fluorescence quantum yields ranging from 0.38 to 0.78 in solution and 0.42 to 0.69 in thin films.<sup>21</sup> Among tetraarylpyrenes, 1,3,5,9-tetrasubstituted pyrenes,<sup>22</sup> 4,5,9,10-tetrasubstituted pyrenes,<sup>23,24</sup> and 1,3,6,8-tetrasubstituted pyrenes<sup>25-27</sup> were studied. The inclusion of tri- and tetrasubstituted phenyl derivatives onto the pyrene backbone yields amorphous materials with only modest photoluminescence quantum yields of 0.28–0.38 in solution (0.24–0.44 in solid state),<sup>25</sup> which highlights the importance of substituent selection in determining the photophysical properties. In particular, 1,3,6,8-tetraphenylpyrene (TPP) has raised considerable interest as a blue emitting material for organic light-emitting diode (OLED)<sup>25</sup> and organic light-emitting field-effect transistor (OLEFET)<sup>28</sup> applications. Derivatives of TPP with four of each 7-*tert*-butylpyrene, 9,9-bis(3-methylbutyl)-9H-fluoren-2-yl, or 4-methoxyphenyl substituents yield materials

<sup>a</sup> Department of Chemistry, American University of Beirut, Beirut 1107-2020, Lebanon. E-mail: bilal.kaafarani@aub.edu.lb

<sup>b</sup> NanoTecCenter Weiz Forschungsgesellschaft mbH, Franz-Pichler-Straße 32, A-8160 Weiz, Austria

<sup>c</sup> Department of Biology & Chemistry, New Mexico Highlands University, Las Vegas, NM 87701, USA

<sup>d</sup> Department of Chemistry and Center for Photochemical Sciences, Bowling Green State University, Bowling Green, Ohio, 43403, USA

<sup>e</sup> Department of Natural Sciences, Lebanese American University, Byblos, Lebanon. E-mail: brigitte.wex@lau.edu.lb

<sup>f</sup> Solar & Photovoltaics Engineering Research Center, Physical Science and Engineering Division, King Abdullah University of Science & Technology, Thuwal 23955-6900, Kingdom of Saudi Arabia

<sup>g</sup> Institute of Solid State Physics, Graz University of Technology, A-8010 Graz, Austria

† Electronic supplementary information (ESI) available. CCDC 1044326, 1015953, 1011328, 1011330, 1015949 and 1039264. For ESI and crystallographic data in CIF or other electronic format see DOI: 10.1039/c5tc02849c

with high fluorescence quantum yields of 0.75–0.99 in dichloromethane solution.<sup>26</sup> In a complex OLED configuration including electron transport layer (ETL) and hole transport layer (HTL), the compound 1,3,6,8-tetrakis[4,2,2-(diphenylvinyl)phenyl]pyrene<sup>29</sup> was utilized as an emitter and showed a turn-on voltage of 3.51 V, a max. luminance of 103 835 cd m<sup>-2</sup> with a max. current efficiency of 5.19 cd A<sup>-1</sup> highlighting the importance of pyrene derivatives for OLED application. However, there is a marked absence of a systematic study of the substitution pattern. Herein, we report the study of structure–property relationships of nine compounds; eight 1,3,6,8-tetraphenylpyrenes embellished with electron donating and electron withdrawing substituents, specifically on the four phenyl rings and of one 1,3,6,8-tetrathiophen-2-ylpyrene. We further report the X-ray crystal structures of six compounds (1, 2, 4, 5, 7, and 9) and importantly explore device characteristics in OLED geometries for compounds 2, 3, 4, and 7.

## Experimental section

Chemicals, solvents, standard grade silica gel (60 Å, 32–63 μm), and silica gel plates (200 μm) were purchased from commercial sources. The reactions that required anhydrous conditions were carried out under argon in oven-dried glassware. CDCl<sub>3</sub> was the solvent for NMR acquired on a 500 MHz Bruker NMR machine and chemical shifts relative to TMS at 0.00 ppm are reported in parts per million (ppm) on the δ scale. Melting points (*T*<sub>m</sub>) were determined using an automatic digital melting point meter (Krüss M5000). Decomposition temperatures (*T*<sub>d</sub>) were determined using a NETZSCH thermogravimetric analyzer.

## Materials and methods

### Synthesis

**1,3,6,8-tetrabromopyrene<sup>30</sup> and tetrakis(triphenylphosphine)-palladium(0)<sup>31</sup> were synthesized according to literature procedures.** Compounds 1, 3, 6, and 7 were synthesized according to a common literature procedure.<sup>27</sup> 1,3,6,8-Tetrabromopyrene (0.50 g, 0.97 mmol) and the corresponding boronic acid (5.82 mmol) were added to 30 mL of toluene followed by 3 mL of 2 M aqueous K<sub>2</sub>CO<sub>3</sub>, and a catalytic amount of tetrabutylammonium bromide. The mixture was purged with argon for 20 min, before tetrakis(triphenylphosphine)-palladium(0) (67 mg, 0.057 mmol) was added and the mixture was stirred at 110 °C for 48 h for compounds 1 and 3 while for 72 h for compounds 6 and 7. After evaporation of the solvent under reduced pressure, the obtained solid was triturated with chloroform using a Soxhlet extraction apparatus. The chloroform extract was then washed with 5% K<sub>2</sub>CO<sub>3</sub> aqueous solution (2 × 50 mL) followed by brine (2 × 50 mL). The organic phase was dried over MgSO<sub>4</sub> and filtered, and the solvent was removed under reduced pressure. Note, due to insolubility, compound 6 was directly obtained by filtration at this stage.

**1,3,6,8-Tetrakis(4-(*tert*-butyl)phenyl)pyrene (1).** The obtained beige solid was then purified by column chromatography starting with hexanes as the mobile phase, and then increasing the polarity to 5% dichloromethane in hexanes to obtain the desired

product, which was then recrystallized from toluene first, then from chloroform to yield 1 (0.50 g, 70%) as a shiny white solid. <sup>1</sup>H NMR (500 MHz, CDCl<sub>3</sub>): δ 8.14 (s, 4H), 7.97 (s, 2H), 7.55 (d, *J* = 8.5 Hz, 8H), 7.49 (d, *J* = 8.5 Hz, 8H), 1.35 (s, 36H). <sup>13</sup>C NMR (125 MHz, CDCl<sub>3</sub>): δ 150.1, 138.1, 136.9, 130.3, 129.5, 129.0, 128.0, 126.0, 125.2, 34.6, 31.4. Anal. calcd for C<sub>56</sub>H<sub>58</sub>: C, 92.00; H, 8.00. Found: C, 91.97; H, 8.06. *T*<sub>m</sub> > 410.0 °C, *T*<sub>d</sub> = 439.1 °C.

**1,3,6,8-Tetrakis(3,4,5-trimethoxyphenyl)pyrene (3).** The obtained orange solid was recrystallized from toluene to yield 3 (0.40 g, 48%) as yellow crystals. <sup>1</sup>H NMR (500 MHz, CDCl<sub>3</sub>): δ 8.18 (s, 4H), 7.97 (s, 2H), 6.80 (s, 8H), 3.90 (s, 12H), 3.84 (s, 24H). <sup>13</sup>C NMR (125 MHz, CDCl<sub>3</sub>): δ 153.1, 137.4, 137.2, 136.4, 128.9, 128.1, 125.8, 125.3, 107.8, 61.0, 56.3. Anal. calcd for C<sub>52</sub>H<sub>50</sub>O<sub>12</sub>: C, 72.04; H, 5.81. Found: C, 71.85; H, 5.84. *T*<sub>m</sub> = 325.0 °C, *T*<sub>d</sub> = 408.7 °C.

**1,3,6,8-Tetrakis(3,5-difluorophenyl)pyrene (6).** The obtained dark green insoluble solid was recrystallized from 1,2-dichlorobenzene to yield 6 (0.25 g, 40%) as shiny yellow greenish needle-like crystals. No NMR data could be collected due to insolubility. Anal. calcd for C<sub>40</sub>H<sub>18</sub>F<sub>8</sub>: C, 73.85; H, 2.79. Found: C, 73.67; H, 2.69. *T*<sub>m</sub> > *T*<sub>d</sub> = 368.2 °C.

**1,3,6,8-Tetrakis(3,5-bis(trifluoromethyl)phenyl)pyrene (7).** The obtained solid was recrystallized from chlorobenzene to yield 7 (0.68 g, 67%) as a shiny white solid. <sup>1</sup>H NMR (500 MHz, CDCl<sub>3</sub>): δ 8.05 (s, 8H), 8.03 (s, 4H), 7.99 (s, 4H), 7.95 (s, 2H); <sup>13</sup>C NMR (125 MHz, CDCl<sub>3</sub>): δ 142.1, 135.1, 132.6 (q, <sup>2</sup>*J*<sub>C-F</sub> = 32.5 Hz), 130.5, 129.5, 128.8, 126.5 (q, <sup>1</sup>*J*<sub>C-F</sub> = 271.3 Hz), 125.8, 125.5, 121.9. Anal. calcd for C<sub>48</sub>H<sub>18</sub>F<sub>24</sub>: C, 54.87; H, 1.73. Found: C, 54.90; H, 1.61. *T*<sub>m</sub> = 314.7 °C, *T*<sub>d</sub> = 318.4 °C.

Compounds 2, 4,<sup>32</sup> and 5<sup>33</sup> were synthesized according to a common literature procedure.<sup>34</sup>

1,3,6,8-Tetrabromopyrene (0.50 g, 0.97 mmol) was added to 20 mL of *n*-propanol, then the corresponding boronic acid (4.27 mmol) was added. The mixture was purged with argon for 20 min, after which palladium(II) acetate (0.70 mg, 3.12 μmol), triphenylphosphine (2.47 mg, 9.42 μmol), and 0.56 mL of 2 M aqueous K<sub>2</sub>CO<sub>3</sub> solution were added, followed by 0.34 mL of deionized water. The mixture was refluxed for 36 h under argon atmosphere and in the dark. The reaction was cooled to room temperature, quenched with water and extracted with ethyl acetate. The combined organic layer was washed with a 5% aqueous K<sub>2</sub>CO<sub>3</sub> solution and a brine solution, and solvent was removed under reduced pressure.

**1,3,6,8-Tetrakis(4-phenoxyphenyl)pyrene (2).** The obtained yellow needle-like crystals were purified by column chromatography starting with hexanes as the mobile phase, and then increasing the polarity to 5% dichloromethane in hexanes to obtain 2 (0.42 g, 49%) as a white solid. <sup>1</sup>H NMR (500 MHz, CDCl<sub>3</sub>): δ 8.14 (s, 4H), 7.94 (s, 2H), 7.57 (d, *J* = 8.5 Hz, 8H), 7.34 (t, *J* = 8.0 Hz, 8H), 7.12 (d, *J* = 8.5 Hz, 8H), 7.08–7.06 (m, 12H). <sup>13</sup>C NMR (125 MHz, CDCl<sub>3</sub>): δ 157.1, 156.8, 136.6, 135.9, 131.9, 129.8, 129.0, 128.1, 126.0, 125.2, 123.5, 119.1, 118.6. Anal. calcd for C<sub>64</sub>H<sub>42</sub>O<sub>4</sub>: C, 87.85; H, 4.84. Found: C, 87.91; H, 4.96. *T*<sub>m</sub> = 276.1 °C, *T*<sub>d</sub> = 503.6 °C.

**1,3,6,8-Tetrakis(4-(methylthio)phenyl)pyrene (4)<sup>32</sup>.** The obtained solid was recrystallized from toluene to yield 4 as a yellow solid (1.00 g, 29%). <sup>1</sup>H NMR (500 MHz, CDCl<sub>3</sub>): δ 8.09 (s, 4H), 7.89 (s, 2H), 7.53 (d, *J* = 8.0 Hz, 8H), 7.37 (d, *J* = 8.0 Hz, 8H),

2.52 (s, 12H).  $^{13}\text{C}$  NMR (125 MHz,  $\text{CDCl}_3$ ):  $\delta$  137.7, 136.6, 131.0, 129.4, 129.05, 128.1, 126.4, 126.0, 125.2, 15.85. Anal. calcd for  $\text{C}_{44}\text{H}_{34}\text{S}_4$ : C, 76.48; H, 4.96; S, 18.56. Found: C, 76.60; H, 5.09; S, 18.41.  $T_m = 318.5$  °C,  $T_d = 392.4$  °C.

**1,3,6,8-Tetrakis(4-fluorophenyl)pyrene (5)**<sup>33</sup>. The obtained greenish solid was recrystallized from toluene to yield **5** (0.70 g, 24%) as yellow crystals.  $^1\text{H}$  NMR (500 MHz,  $\text{CDCl}_3$ ):  $\delta$  8.05 (s, 4H), 7.87 (s, 2H), 7.56 (dd,  $^3J_{\text{H-H}} = 8.5$  Hz,  $^3J_{\text{H-F}} = 5.5$  Hz, 8H), 7.17 (d,  $J = 8.5$  Hz, 8H).  $^{13}\text{C}$  NMR (125 MHz,  $\text{CDCl}_3$ ):  $\delta$  163.4 (d,  $^1J_{\text{C-F}} = 245$  Hz), 136.7 (d,  $^4J_{\text{C-F}} = 2.5$  Hz), 136.3, 132.1 (d,  $^3J_{\text{C-F}} = 7.5$  Hz), 129.6, 128.2, 125.8, 125.3, 115.5 (d,  $^2J_{\text{C-F}} = 20$  Hz). Anal. calcd for  $\text{C}_{40}\text{H}_{22}\text{F}_4$ : C, 83.03; H, 3.83. Found: C, 82.92; H, 4.01.  $T_m = 309.0$  °C,  $T_d = 381.8$  °C.

Compounds **8**<sup>35</sup> and **9**<sup>36</sup> were synthesized according to a literature procedure.<sup>30</sup>

**Tetramethyl 4,4',4'',4'''-(pyrene-1,3,6,8-tetrayl)tetrabenzoate (8)**<sup>35</sup>. Yellow solid **8** (3.00 g, 73%).  $^1\text{H}$  NMR (500 MHz,  $\text{CDCl}_3$ ):  $\delta$  8.15 (d,  $J = 8.0$  Hz, 8H), 8.07 (s, 4H), 7.92 (s, 2H), 7.67 (d,  $J = 8.0$  Hz, 8H), 3.91 (s, 12H).  $^{13}\text{C}$  NMR (125 MHz,  $\text{CDCl}_3$ ):  $\delta$  166.9, 145.35, 136.5, 130.6, 129.7, 129.2, 129.2, 128.3, 125.7, 125.5, 52.3. Anal. calcd for  $\text{C}_{48}\text{H}_{34}\text{O}_8$ : C, 78.04; H, 4.64. Found: C, 78.31; H, 4.77.  $T_m = 345.8$  °C,  $T_d = 410.0$  °C.

**1,3,6,8-Tetrakis(thiophen-2-yl)pyrene (9)**<sup>36</sup>. Light orange solid **9** (0.78 g, 17%).  $^1\text{H}$  NMR (500 MHz,  $\text{CDCl}_3$ ):  $\delta$  8.45 (s, 4H), 8.17 (s, 2H), 7.46 (dd,  $J = 5.0, 1.0$  Hz, 4H), 7.34 (dd,  $J = 3.5, 1.0$  Hz, 4H), 7.20 (dd,  $J = 5.0, 3.5$  Hz, 4H).  $^{13}\text{C}$  NMR (125 MHz,  $\text{CDCl}_3$ ):  $\delta$  141.8, 131.2, 129.7, 129.1, 128.35, 127.5, 126.5, 125.8, 125.7. Anal. calcd for  $\text{C}_{32}\text{H}_{18}\text{S}_4$ : C, 72.42; H, 3.42; S, 24.17. Found: C, 72.33; H, 3.28; S, 24.06.  $T_m = 306.4$  °C (Lit.<sup>36</sup> 308.0 °C),  $T_d = 400.1$  °C.

### Electrochemical analysis

The electrochemical measurements were carried out under an inert atmosphere in dry deoxygenated dichloromethane (DCM) solution containing 0.1 M tetrabutylammonium hexafluorophosphate as an electrolyte. A CH-Instrument 620D potentiostat equipped with a conventional three-electrode cell utilizing a glassy carbon working electrode, a platinum wire counter electrode, and a silver wire coated with silver chloride as the pseudo-reference electrode, was used for the measurements. The potentials were referenced to the decamethylferrocene/decamethylferrocenium (DMFc/DMFc<sup>+0</sup>) couple by using decamethylferrocene as an internal standard. All measured potentials were converted to the ferrocene/ferrocenium scale; (DMFc/DMFc<sup>+0</sup>) was measured to be  $-0.54$  vs. FcCp<sub>2</sub><sup>+0</sup> in DCM.

### Computational details

Ground-state molecular geometries and vibrational frequencies of isolated compounds **1–9** were determined at the density functional theory (DFT) level, using the B3LYP functional and the 6-31G(d,p) basis set. Vertical first electronic singlet excited states were explored at the time-dependent (TD) DFT and Tamm–Dancoff approximation (TDA) levels using the B3LYP functional and, the range-separated hybrid functional  $\omega\text{B97}^{37}$  were chosen. In all instances, the 6-31G(d,p) basis set was applied. For the  $\omega\text{B97}$  functional, the  $\omega$  value for each compound was tuned with respect to the ionization potential (IP-tuning) by

minimizing  $J(\omega)$  in eqn (1) where  $\epsilon_{\text{HOMO}}^{\omega}(N)$  is the HOMO energy of the neutral molecule (with  $N$  electrons) and  $E_{\text{gs}}(\omega, N)$  and  $E_{\text{gs}}(\omega, N - 1)$  represent the total energy of the neutral molecule and the cation, respectively.<sup>38</sup>

$$J(\omega) = |\epsilon_{\text{HOMO}}^{\omega} - (E_{\text{gs}}(\omega, N) - E_{\text{gs}}(\omega, N - 1))| \quad (1)$$

The following omega ( $\omega$ ) values were obtained: 0.148 (**1**); 0.143 (**2**); 0.145 (**3**); 0.149 (**4**); 0.162 (**5**); 0.162 (**6**); 0.155 (**7**); 0.150 (**8**); 0.165 (**9**); 0.162 (TPP); 0.248 (pyrene). The polarizable continuum model (PCM) in its integral equation formalism variant (IEFPCM) was used at the TDDFT level to explore the first singlet electronic excited states of **1–9**, TPP and pyrene in tetrahydrofuran. All calculations were carried out using the Gaussian 09 (Revision D.01) software.<sup>39</sup>

### Photophysical studies in solution

The absorption, fluorescence excitation and emission spectra were acquired for **1–9** using 100  $\mu\text{M}$  (for UV-visible measurements) and 1–2  $\mu\text{M}$  (for fluorescence measurements) of each compound prepared in different solvents. For UV-visible spectral measurements a JASCO V-570 UV-NIR spectrophotometer was used, whereas fluorescence measurements were done using a Jobin-Yvon-Horiba Fluorolog III spectrofluorometer. The excitation source was a 100 W xenon lamp and the slit width was fixed at 5 nm for all measurements. The fluorescence lifetime was measured using the same instrument. The fluorescence quantum yields ( $\Phi_f$ ) were evaluated according to the following eqn (2):

$$\Phi_{\text{unk}} = \Phi_{\text{std}} \frac{F_{\text{unk}} A_{\text{std}} n_{\text{unk}}^2}{F_{\text{std}} A_{\text{unk}} n_{\text{std}}^2} \quad (2)$$

where standard (std) refers to the reference sample (*i.e.* 9,10-diphenyl anthracene in cyclohexane) and unknown (unk) refers to compounds (**1–9**), wherein, the quantum yield of 9,10-diphenylanthracene in cyclohexane was taken as 1.0.  $F$  corresponds to the integrated intensity of the emission spectra of the sample or reference, while  $A$  is the optical density of the sample or reference at the excitation wavelength. Finally,  $n$  is the refractive index of the solvent being used.<sup>40</sup> All fluorescence quantum yields and lifetime measurements were carried out under nitrogen atmosphere.

### Photophysical studies in solid state

The absolute fluorescence quantum yields in crystalline solids and thin films were acquired on a Hamamatsu Quantaurus-QY (C11347) instrument equipped with a CCD multichannel detector, an integrating sphere and xenon lamp excitation.

### X-ray crystal structure analysis

The X-ray diffraction experiments were carried out using a Bruker SMART APEX II CCD diffractometer, with Mo K $\alpha$  radiation ( $\lambda = 0.71073$  Å) at 100 K for compounds **1, 2, 5, 7** and **9**, and at 297 K for compound **4**, while no suitable crystals were obtained for the remaining materials. The raw data frames were integrated with the SAINT+ program using a narrow-frame algorithm.<sup>41</sup> Absorption corrections were applied using the semi-empirical method of the SADABS program.<sup>42</sup> The structures were solved by direct methods and refined using Olex2<sup>43</sup>

by full-matrix least-squares methods on  $F^2$  using SHELXL-97 in anisotropic approximation for all non-hydrogen atoms. The main crystallographic data are summarized in Table 6. CIF files of compounds **1**, **2**, **4**, **5**, **7**, and **9** have been deposited and allocated the following CCDC 1044326, 1015953, 1011328, 1011330, 1015949 and 1039264, respectively.

### Organic light-emitting devices and characterization

The electroluminescence characteristics of the new compounds were investigated in devices featuring them as the active layer in a standard sandwich geometry: indium tin oxide (ITO)/poly(3,4-ethylenedioxythiophene)-poly-styrenesulfonic acid (Baytron P VPAI 4083) (PEDOT:PSS)/**2**, **3**, **4** and **7**/Ca/Al. ITO-covered glass substrates were first carefully rinsed with deionized water, acetone and isopropyl alcohol. Afterwards the substrates were subjected to various ultrasonic treatments in detergent, deionized water, acetone, and isopropanol. A dry cleaning step in oxygen plasma finished the cleaning procedure while at the same time providing an enhancement of the surface wettability of PEDOT:PSS. Consecutively, a layer of PEDOT:PSS was applied *via* spin-coating under ambient conditions and dried under ambient conditions at 200 °C for 5 min. The active layers were evaporated at a rate of 0.6 Å s<sup>-1</sup> from a resistively heated crucible under dynamic vacuum at an initial base pressure lower than  $1.0 \times 10^{-6}$  mbar. The layer thicknesses were controlled using a quartz-crystal microbalance and verified using a Veeco Dimension V atomic force microscope equipped with a Nanoscope V controller in tapping mode at several positions. The resulting layer thickness amounted to 80 nm. The cathode materials (Ca, Al) were deposited onto the substrate with thicknesses of 10 nm and 100 nm for Ca and Al, respectively, without breaking the vacuum through a shadow mask. Consequently, multiple devices with a device-area of 10 mm<sup>2</sup> were formed on a single substrate. Electroluminescence (EL) spectra were acquired using an ORIEL spectrometer with an attached calibrated charge-coupled device (CCD) camera. Current–luminance–voltage ( $I$ – $L$ – $V$ ) characteristics were recorded in a customized setup using a Keithley 2612A source measure unit for recording the  $I$ – $V$  characteristics while the luminance was measured using a Keithley 6517 electrometer using a photodiode calibrated by a Konica-Minolta LS-100 luminance meter.

## Results and discussion

### Synthesis

Electrophilic aromatic substitution of the commercially available pyrene in the presence of nitrobenzene afforded 1,3,6,8-tetrabromopyrene (Py-Br<sub>4</sub>) in 98% yield.<sup>44</sup> Suzuki coupling of Py-Br<sub>4</sub><sup>30</sup> with a series of electron-rich and electron-poor phenyl boronic acids yielded *p*-*tert*-butyl **1**, *p*-phenoxy **2**, 3',4',5'-trimethoxy **3**, and methylthio **4**,<sup>32</sup> and *p*-fluoro **5**,<sup>33</sup> 3,5-difluoro **6**, 3,5-trifluoromethyl **7**, methoxycarbonyl **8**,<sup>45</sup> respectively. In addition, the reaction of Py-Br<sub>4</sub> with 2-thiophene boronic acid yielded 1,3,6,8-tetrathienylpyrene **9**, Scheme 1. Compounds **2**, **3**, and **6** are new compounds, while compounds **1**<sup>46,47</sup> and **7**<sup>48,49</sup> have previously

been reported only in a proceeding and patent applications leaving experimental data inaccessible. Several Suzuki–Miyaura cross-coupling procedures with a variety of solvents such as toluene,<sup>27</sup> *n*-propanol<sup>34</sup> or 1,4-dioxane (dioxane)<sup>30</sup> were tested. The procedure invoking toluene was found to be the most suitable in the synthesis of **1**, **3**, **6**, and **7**. *n*-Propanol was found to be the solvent of choice for the synthesis of compounds **2**, **4** and **5**, while dioxane was found to be the preferred solvent for the preparation of **8** and **9**.

### Photophysical studies

Pyrene is a well-characterized chromophore with four absorption bands as observed in a cyclohexane solution; a low energy electronic transition  $S_0 \rightarrow S_1$  at 372 nm ( $\epsilon = 510 \text{ mol}^{-1} \text{ cm}^{-1} \text{ L}$ ) with a vibrational fine structure, followed by higher energy electronic  $S_0 \rightarrow S_2$ ,  $S_0 \rightarrow S_3$  and  $S_0 \rightarrow S_4$  transitions at 334 ( $\epsilon = 55\,000 \text{ mol}^{-1} \text{ cm}^{-1} \text{ L}$ ), 272 ( $\epsilon = 54\,000 \text{ mol}^{-1} \text{ cm}^{-1} \text{ L}$ ), and 243 nm ( $\epsilon = 88\,000 \text{ mol}^{-1} \text{ cm}^{-1} \text{ L}$ ), respectively.<sup>19</sup> According to the Platt nomenclature, the two lowest-lying  $\pi \rightarrow \pi^*$  transitions lead to excited states  $L_a$  and  $L_b$ .  $L_a$  is due to a HOMO–LUMO excitation polarized along the long axis of pyrene, while  $L_b$  is due to degenerate HOMO–1  $\rightarrow$  LUMO and HOMO  $\rightarrow$  LUMO+1 configurations polarized along the short axis of pyrene.<sup>49</sup>  $L_b$  is the lowest energy  $S_0 \rightarrow S_1$  transition and is symmetry forbidden. A low fluorescence quantum yield for pyrene is thus observed. The second transition  $L_a$ , also referred to as  $S_0 \rightarrow S_2$  energy transition, is symmetry allowed and characterized by a large oscillator strength. A modulation of the fluorescence quantum yield hinges on lowering of the energy level of this transition compared to  $L_b$ . Substitution in positions 2 and 7 does not result in a change of the molecular orbital levels due to the presence of a nodal plane along these positions. A substitution on positions 1, 1 and 6, 1 and 8, and 4 and 9<sup>50</sup> in pyrene, however, modulates the allowed transition and thus results in materials with a large oscillator strength for the  $S_0 \rightarrow S_1$  transition and high fluorescence quantum yields.<sup>51</sup> 1,3,6,8-Tetraphenylpyrene (TPP) shows a marginal loss of features in both absorption and fluorescence spectra coupled to a red shift in absorption and fluorescence spectra.<sup>8,52</sup> TPP shows an increased fluorescence quantum yield of 0.73 compared to 0.29 for pyrene in degassed THF solution. The significant increase is additionally attributed to steric inhibition of excimer formation.<sup>53</sup> Even though the intersystem crossing rate ( $k_{\text{ISC}}$ ) increased from  $0.16 \times 10^7 \text{ s}^{-1}$  to  $3.7 \times 10^7 \text{ s}^{-1}$ , the fluorescence rate constant ( $k_f$ ) value increased from  $0.25 \times 10^7 \text{ s}^{-1}$  to  $33.3 \times 10^7 \text{ s}^{-1}$  going from the planar pyrene molecule to the non-planar TPP.<sup>53</sup> In particular, in vacuum deposited thin films, TPP shows a high photoluminescence quantum efficiency of  $68 \pm 3\%$ .<sup>33</sup> In the present case, we aim to deduce the effect of introducing electron donating and electron withdrawing substituents on the four phenyl rings of TPP on the photophysical properties.

The normalized UV-visible absorption and fluorescence spectra of compounds **1**–**9** in chloroform are shown in Fig. 1. All compounds showed two transitions: one in the region 350–440 nm for the  $S_0 \rightarrow S_1$  absorption transition and the other in the region 250–330 nm for the  $S_0 \rightarrow S_n$  ( $n > 1$ ) absorption. The shift in comparison to TPP as a reference



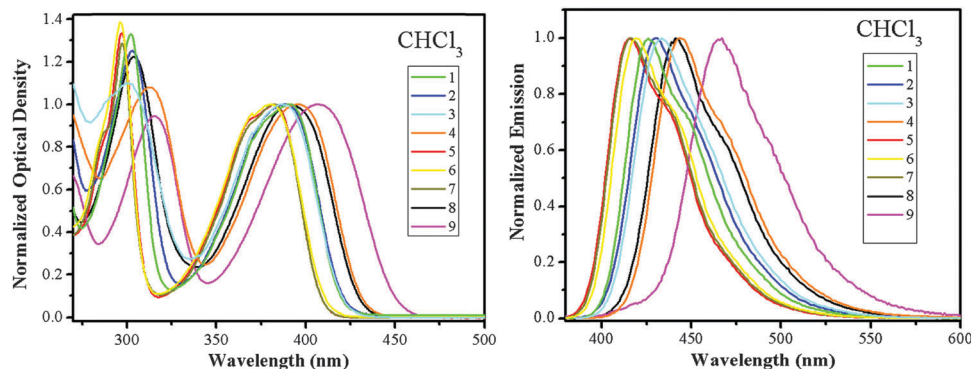


Fig. 1 Normalized absorption (left) and normalized emission (right) spectra of compounds **1–9** in chloroform.

Table 1 Photophysical data in chloroform<sup>a</sup>

Compound	$\lambda_{\text{max}}^{\text{em}}$ (in nm)	$\lambda_{\text{max}}^{\text{abs}}$ (in nm)	$\Delta\lambda$ (in $\text{cm}^{-1}$ )	$\tau$ (in ns)	$\phi_{\text{F}}$	$k_{\text{r}}$ (in $10^8$ ) $\text{s}^{-1}$	$k_{\text{nr}}$ (in $10^8$ ) $\text{s}^{-1}$
<b>1</b>	426	391	2101	1.83	0.97	5.30	0.16
<b>2</b>	430	388	2517	1.86	0.98	5.27	0.11
<b>3</b>	434	387	2798	1.75	0.85	4.86	0.86
<b>4</b>	444	396	2730	1.66	0.8	4.82	1.20
<b>5</b>	416	382	2140	2.27	0.84	3.70	0.70
<b>6</b>	419	380	2449	1.93	0.75	3.89	1.30
<b>7</b>	416	382	2140	2.02	0.88	4.36	0.59
<b>8</b>	443	391	3002	1.93	0.89	4.61	0.57
<b>9</b>	467	407	3157	0.54	0.17	3.15	15.4

<sup>a</sup>  $\lambda_{\text{max}}^{\text{em}}$ : emission maximum;  $\lambda_{\text{max}}^{\text{abs}}$ : absorption maximum;  $\Delta\lambda$ : Stokes shift;  $\tau$ : fluorescence lifetime;  $\phi_{\text{F}}$ : fluorescence quantum yield;  $k_{\text{r}}$ : radiative rate constant and  $k_{\text{nr}}$ : non-radiative rate constant.

fluorine substituents exhibited a negligible 2 nm (0.01 eV) hypsochromic shift in fluorescence in THF. The extent of bathochromic shift in THF increased from **7**, **6**, **1**, and **2** with  $<0.1$  eV to **3**, **4**, **8**, and **9** with  $>0.1$  eV, Table 2. The structural features in the fluorescence spectra were also lost in **2**, **3**, **8**, and **9** and relatively resolved in **1**, **4**, **5**, **6**, and **7**. To make sure that these structural features are not due to excimer formation as commonly observed in pyrene or dimer formation as observed for TPP,<sup>55</sup> we measured the emission spectra at different excitation wavelengths in the 350–450 nm range in chloroform for all the compounds; no changes in the positions of the emission spectra were observed except for a variation in fluorescence intensity due to changes in absorbance at these excitation wavelengths. This suggests that there is only one emitting species in all the compounds. Similarly, when the excitation spectra were recorded at various possible emission wavelengths in the 390–540 nm range, no changes in the spectral positions in the excitation spectra were found. This rules out any possible excimer formation in these compounds at the studied concentration. The representative absorption, excitation and emission spectra for compound **5** (with structural feature in the spectrum) and **9** (without any structural feature in the spectrum) are summarized in Fig. 2 (for other compounds, see the ESI†). The excitation spectra for these compounds look similar to their respective absorption spectra, even the structural features could be seen in the excitation spectra for compounds **1**, **5**, and **7** similar to their absorption spectra. The fluorescence spectra were also found to be mirroring the absorption spectra. From these

observations, it can be concluded that both the absorbing and emitting species are the same for all these compounds. Therefore, the absorption and fluorescence spectral changes among different compounds are due to a fine balance between conformational effects and electronic effects linked to the substitution of the phenyl units by electron-rich groups.<sup>25</sup>

From the shape of absorption and fluorescence spectra, such as relatively resolved structural features for **5**, **6** and **7** and completely structureless features for **8** and **9**, it can be concluded that these compounds exhibit a noticeable conformational disorder associated with the rotation of the external rings. This interpretation is consistent with the earlier observation by Moorthy *et al.*<sup>25</sup> who restricted the rotation of the external rings by substituting methyl groups at the two *ortho*-positions of the phenyl group and found well-resolved absorption and fluorescence spectra in dichloromethane.<sup>25</sup> Stokes shifts ( $\Delta\lambda$ ) along with absorption and emission maxima for compounds **1–9** in chloroform are summarized in Table 1. Compounds **8** and **9** have the largest Stokes shifts, whereas compounds **1**, **5**, **6** and **7** have the smallest (ESI†). This reflects a trend similar to that found for the structural features of the compounds, thus, suggesting that rotation of the external rings plays a significant role in the spectral properties though restriction of rotation could be influenced by the electronic effects. For instance, the electron-donating nature of substituents in **1** and the electron-withdrawing nature in **5**, **6** and **7** might create a partial double bond character (extending the conjugation of the pyrene moiety into the phenyl group) thus restricting rotation. At the same

Table 2 Photophysical data in various solvents<sup>a</sup>

Compound	Solvent	$\lambda_{\text{max}}^{\text{em}}$ (nm)	$\lambda_{\text{max}}^{\text{abs}}$ (nm)	$\Delta\lambda$ (cm <sup>-1</sup> )	$\tau$ (ns)	$\phi_{\text{F}}$	$k_{\text{r}}$ (10 <sup>8</sup> ) s <sup>-1</sup>	$k_{\text{nr}}$ (10 <sup>8</sup> ) s <sup>-1</sup>
1	Chloroform	426	391	2101	1.83	0.97	5.30	0.16
1	DMF	428	393	2081	1.92	0.89	4.64	0.57
1	THF	424	390	2056	1.94	0.90	4.64	0.52
1	DMSO	—	—	—	—	—	—	—
1	1,4-Dioxane	425	389	2178	1.89	0.82	4.34	0.95
1	Cyclohexane	423	387	2199	1.89	0.81	4.29	1.01
2	Chloroform	430	388	2517	1.86	0.98	5.27	0.11
2	DMF	432	391	2427	1.94	0.91	4.69	0.46
2	THF	429	389	2397	1.91	0.998	5.23	0.01
2	DMSO	434	387	2798	1.84	0.69	3.75	1.68
2	1,4-Dioxane	429	389	2397	1.86	0.85	4.57	0.81
2	Cyclohexane	425	384	2512	1.85	0.79	4.27	1.14
3	Chloroform	434	387	2798	1.75	0.85	4.86	0.86
3	DMF	438	392	2679	1.99	0.83	4.17	0.85
3	THF	434	389	2665	1.88	0.75	3.99	1.33
3	DMSO	440	395	2589	1.95	0.78	4.00	1.13
3	1,4-Dioxane	432	388	2625	1.83	0.75	4.10	1.37
3	Cyclohexane	432	384	2894	1.75	0.93	5.31	0.40
4	Chloroform	444	396	2730	1.66	0.80	4.82	1.20
4	DMF	447	400	2629	1.73	0.73	4.22	1.56
4	THF	442	396	2628	1.63	0.72	4.42	1.72
4	DMSO	450	403	2592	1.71	0.68	3.98	1.87
4	1,4-Dioxane	441	396	2577	1.58	0.72	4.56	1.77
4	Cyclohexane	437	396	2369	1.47	0.47	3.20	3.61
5	Chloroform	416	382	2140	2.27	0.84	3.70	0.70
5	DMF	417	384	2061	2.34	0.87	3.72	0.56
5	THF	415	383	2013	2.51	0.81	3.23	0.76
5	DMSO	421	387	2087	2.13	0.84	3.94	0.75
5	1,4-Dioxane	415	383	2013	2.44	0.82	3.36	0.74
5	Cyclohexane	413	381	2034	2.74	0.83	3.03	0.62
6	Chloroform	419	380	2449	1.93	0.75	3.89	1.30
6	DMF	425	381	2717	2.11	0.80	3.79	0.95
6	THF	422	383	2413	2.09	0.81	3.88	0.91
6	DMSO	427	386	2488	1.93	0.68	3.52	1.66
6	1,4-Dioxane	419	382	2312	2.03	0.80	3.94	0.99
6	Cyclohexane	415	379	2289	2.12	0.72	3.40	1.32
7	Chloroform	416	382	2140	2.02	0.88	4.36	0.59
7	DMF	427	386	2488	2.13	0.91	4.27	0.42
7	THF	420	383	2300	2.14	0.85	3.97	0.70
7	DMSO	427	387	2421	2.07	—	—	—
7	1,4-Dioxane	419	382	2312	2.08	0.80	3.85	0.96
7	Cyclohexane	413	382	1965	2.18	0.93	4.27	0.32
8	Chloroform	443	391	3002	1.93	0.89	4.61	0.57
8	DMF	446	393	3024	1.97	0.78	3.96	1.12
8	THF	440	390	2914	1.88	0.75	3.99	1.33
8	DMSO	448	398	2804	1.95	0.57	2.92	2.21
8	1,4-Dioxane	441	390	2965	1.87	0.75	4.01	1.34
8	Cyclohexane	—	—	—	1.78	—	—	—
9	Chloroform	467	407	3157	0.54	0.17	3.15	15.4
9	DMF	470	413	2936	0.56	0.15	2.68	15.2
9	THF	464	408	2958	0.50	0.14	2.80	17.2
9	DMSO	474	416	2941	0.63	0.16	2.54	13.3
9	1,4-Dioxane	466	407	3111	0.47	0.14	2.98	18.3
9	Cyclohexane	460	403	3075	0.47	0.11	2.34	18.9

<sup>a</sup>  $\lambda_{\text{max}}^{\text{em}}$ : emission maximum;  $\lambda_{\text{max}}^{\text{abs}}$ : absorption maximum;  $\Delta\lambda$ : Stokes shift;  $\tau$ : fluorescence lifetime;  $\phi_{\text{F}}$ : fluorescence quantum yield;  $k_{\text{r}}$ : radiative rate constant and  $k_{\text{nr}}$ : non-radiative rate constant.

time, the thienyl moiety in **9** could rotate easily around the single bond making the conjugation between the pyrene moiety and the thienyl group less effective. In the case of **8**, the conjugation between the methylbenzoate group and the pyrene moiety is limited since the conjugation would need to create two negative charges (on oxygen) in the opposite site (two negative charges) and thus would strain the system. This idea of degree of extending the conjugation of the pyrene moiety into the phenyl group among **1**, **5**, **6** and **7** in contrast to **8** and **9**

is further supported by the resolved structural features of **5**, **6** and **7** and structureless features for **8** and **9** as discussed earlier. This is in accordance with the findings of Moorthy *et al.*<sup>25</sup>

The fluorescence quantum yields for compounds **1–9** in chloroform are summarized in Table 1. The fluorescence quantum yield ranged from 75% to 98% for all compounds except for **9** with only 17% yield. No obvious trend was observed. Thiophene rings decrease fluorescence quantum yield when linked to as opposed to fused onto a core,<sup>56</sup> thus leading to a

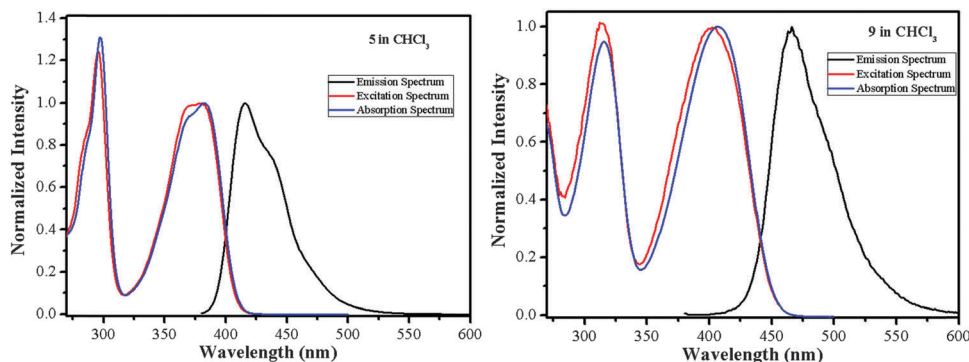


Fig. 2 Normalized absorption, excitation and emission spectra of **5** (left) ( $\lambda_{\text{ex}} = 370$  nm;  $\lambda_{\text{em}} = 440$  nm) and **9** (right) in chloroform ( $\lambda_{\text{ex}} = 370$  nm;  $\lambda_{\text{em}} = 466$  nm).

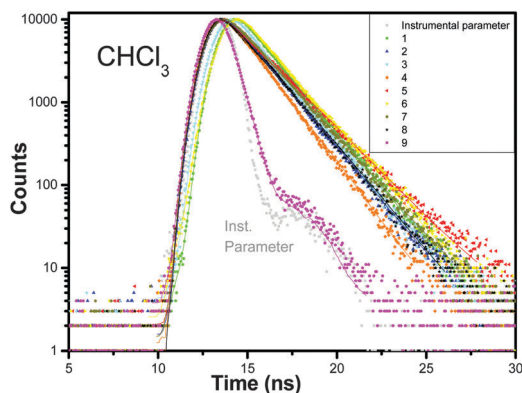


Fig. 3 Time-resolved fluorescence decay profile of compounds **1–9** in chloroform.

relatively low fluorescence quantum yield for compound **9** compared to rest of the compounds. The fluorescence lifetime of these compounds was measured under nitrogen atmosphere and the decay profile is shown in Fig. 3. When the fluorescence lifetime was measured at various possible emission wavelengths keeping the excitation wavelength constant, there was no change in the fluorescence lifetime (see ESI<sup>†</sup>), which further confirms the absence of the excimer. The fluorescence decay profile for all of these compounds in chloroform could be fit to a single exponential decay (see ESI<sup>†</sup>). The presence of a single exponential decay further suggests that emission emanates from a single excited state. The rate constant for radiative decay ( $k_r$ ) was calculated using eqn (3):<sup>40</sup>

$$k_r = \frac{\phi_f}{\tau_f} \quad (3)$$

while  $k_{\text{nr}}$ , *i.e.* the average non-radiative rate constant, was calculated using eqn (4):<sup>40</sup>

$$k_{\text{nr}} = k_{\text{tot}} - k_r \quad (4)$$

The fluorescence lifetimes, rate constants for radiative decay and average non-radiative rate constants for various compounds in chloroform are gathered in Table 1. The fluorescence lifetimes of these compounds were found to be in the 0.5–2.5 ns

range in chloroform as well as in cyclohexane (discussed later on). It should be noted that a significant decrease in the experimental fluorescence lifetime in deaerated THF occurred upon moving from pyrene (322 ns) to TPP (2 ns). The fluorescence lifetime further decreased in substituted TPP (<3 ns) depending on the nature and position of the substituent. The highest lifetime values were attributed to the fluorine containing compounds and the lowest values were attributed to the sulfur containing compounds. The  $k_r$  values were found to be in the order of magnitude of TPP ( $3.33 \times 10^8 \text{ s}^{-1}$ ) and  $k_{\text{nr}}$  values also did not show any trend except for the fact that the  $k_{\text{nr}}$  value was highest for **9** (containing the thiophene aryl component). This is also reflected in the comparably lower  $k_r$ , lifetime and most significantly in the low quantum yield value.

To investigate the solvatochromic behavior of these compounds, six different solvents namely: chloroform, cyclohexane, dimethylsulfoxide, *N,N*-dimethylformamide, 1,4-dioxane, and tetrahydrofuran were selected. All the compounds showed variation in absorption and fluorescence spectra upon changing solvent polarity. Compounds **1** and **8** could not be measured in dimethylsulfoxide and cyclohexane due to poor solubility. Fig. 4 and 5 depict UV-visible absorption and fluorescence spectra of **5** and **9**, respectively. The structural features of both absorption and fluorescence spectra of **5** are retained upon changing the solvent environment. For all the compounds under investigation, it was observed that there is no change in spectral features by changing the solvent environment. However, for all compounds a positive solvatochromism was observed, whereby a red shift was detected in both absorption and fluorescence spectra while increasing the polarity of the solvent, which is expected for a  $\pi$ - $\pi^*$  transition. Sulfur-containing compounds **4** and **9** showed a clear red shift in all solvents in comparison with the other seven compounds in both absorbance and emission spectra. The solvatochromic change of compounds **1–9** with respect to the change in solvent environment could be better understood by evaluating the Stokes shift as listed in Table 2. The correlation of Stokes shift with the solvent environment could be studied as per the theory of general solvent effects and the dielectric continuum theory.<sup>40,56</sup> The plots of Stokes shift *versus*  $\Delta f$  (orientation polarizability) and  $E_{\text{T}}30$  (solvent polarity scale) were generated for all compounds **1–9**. A common feature

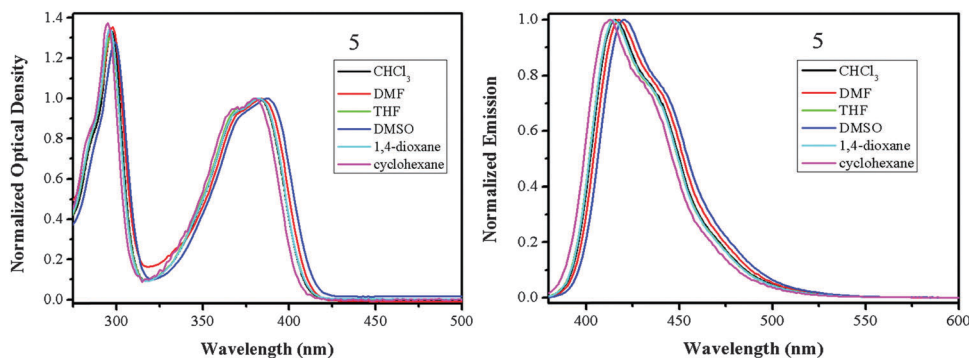


Fig. 4 UV-visible absorption (left) and fluorescence (right) spectra of **5** in different solvents.

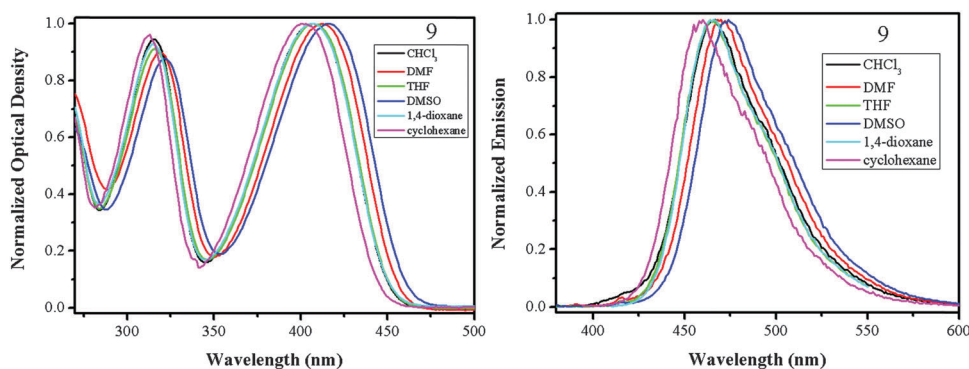


Fig. 5 UV-visible absorption (left) and fluorescence (right) spectra of **9** in different solvents.

of compounds (1–9) is their minimal solvent effect as found by the near zero slope for plots of Stokes shift *versus*  $\Delta f$  and  $E_T30$  (see ESI<sup>†</sup>). In few cases, the vibrationally structured fluorescence spectrum suggests a planar excited-state configuration as the origin of emission. Fused polycyclic aromatic compounds exhibit fluorescence spectra rich in the vibronic structure, wherein a marked absence in the solvatochromic effect is also well established.<sup>18</sup> The fluorescence lifetimes, quantum yields, radiative and non-radiative rate constants for compounds 1–9 are summarized in Table 2. Unlike the UV-visible absorption and fluorescence spectra, these values did not show any systematic trend with solvent polarity. Indeed the estimated values for quantum yields and lifetimes were quite close in most cases and were within the error margin.

### Computational studies

TDDFT with a B3LYP functional needs caution when modelling the lowest singlet excited states in large unsaturated molecules in general, and in pyrene specifically.<sup>19</sup> The B3LYP functional tends to overdelocalize the wavefunctions.<sup>57</sup> It is well noted in the literature that the B3LYP functional overestimates the  $S_0 \rightarrow S_1$  transition and accurately reproduces the  $S_0 \rightarrow S_2$  transition. The reason for this apparent accuracy is ascribed to the cancelation of two errors, the underestimation of the excited-state potential energy curve and the overestimation of the (0, 0) transition due to the computation of the vertical excitation rather than the true (0, 0) transition.<sup>58</sup> It is also important to note that TPP and 1–9 exhibit as the lowest excited state the same characteristics as

the  $S_0 \rightarrow S_2$  transition of pyrene wherein the major contribution is from the HOMO–LUMO nature; the derivatives 1–9 are, despite the small basis set, well described using the  $\omega$ B97 functional. The  $\omega$ B97 functional behaves similar to long-range corrected functionals and in fact exhibits a smaller observed error; however, this functional misses short-range Hartree–Fock exchange, which can potentially give rise to the large error observed for pyrene itself.<sup>59</sup> Time-dependent DFT was used to compute the energies of the vertical transitions in the gas phase and in a solution environment. Table 3 shows the results of TD-DFT and TDA calculations as an overview of vertical transition wavelengths and energies, oscillator strengths as well as transition dipole moments for pyrene, TPP and compounds 1–9 as calculated using B3LYP and  $\omega$ B97 in the gas phase. As expected, all absorptions appear at shorter wavelengths (higher energy) going from the B3LYP-TD to  $\omega$ B97-TD to  $\omega$ B97-TDA level of theory. In all cases, though, the general trends for compounds 1–9 are retained. For all compounds 1–9, as in the TPP case, the  $S_0 \rightarrow S_1$  lowest energy transition is allowed with a high oscillator strength. This transition is similar in nature to the  $S_0 \rightarrow S_2$  transition of pyrene.<sup>5,7</sup> The calculated absorption maxima agree well with experimental data. For all compounds 1–9, the lowest energy  $S_0 \rightarrow S_1$  transition is best described as HOMO  $\rightarrow$  LUMO excitation with more than 95% contribution. When TDA-DFT was applied, the lowest energy transition presents a slight shift to higher energy as well as an increase in oscillator strength. The molecular orbitals involved

**Table 3** Time-dependent (TD) DFT and Tamm–Dancoff approximation (TDA) results for wavelengths ( $\lambda_{\text{vert}}$ , nm), energies ( $E_{\text{vert}}$ , eV), oscillator strengths, and transition dipole moments ( $\mu_{\text{ge}}$ , Debye) for the lowest two transitions in compounds **1–9** in the gas phase

Functional Basis set	B3LYP-TD						$\omega$ B97-TD						$\omega$ B97-TDA								
	6-31G(d,p)						6-31G(d,p)						6-31G(d,p)								
Compound	Transition	$\lambda_{\text{vert}}$ (nm)	$E_{\text{vert}}$ (eV)	$f$	$\mu_{\text{ge}}$ (D)	Electronic configuration	$\lambda_{\text{vert}}$ (nm)	$E_{\text{vert}}$ (eV)	$f$	$\mu_{\text{ge}}$ (D)	Electronic configuration	$\lambda_{\text{vert}}$ (nm)	$E_{\text{vert}}$ (eV)	$f$	$\mu_{\text{ge}}$ (D)	Experiment	$\lambda_{\text{max}}$ THF (nm)	$E_{\text{vert}}$ (eV)	$f$	$\mu_{\text{ge}}$ (D)	
Pyrene	$S_0 \rightarrow S_1$	333	3.72	0.256	2.814	HOMO-1 $\rightarrow$ LUMO (47%)	315	3.94	0.000	0.000	HOMO-1 $\rightarrow$ LUMO (47%)	373	3.93	0.000	0.000	373	310	4.00	0.000	0.000	0.000
	$S_0 \rightarrow S_2$	328	3.78	0.000	0.000	HOMO $\rightarrow$ LUMO+1 (50%)	309	4.02	0.321	3.258	HOMO $\rightarrow$ LUMO+1 (50%)	336	3.96	0.360	3.460	336	292	4.25	0.360	3.460	3.460
TAP	$S_0 \rightarrow S_1$	398	3.11	0.745	9.766	HOMO-1 $\rightarrow$ LUMO (96%)	385	3.22	0.770	9.772	HOMO-1 $\rightarrow$ LUMO (96%)	384	3.23	0.932	11.186	384	364	3.40	0.932	11.186	11.186
	$S_0 \rightarrow S_2$	354	3.51	0.000	0.002	HOMO-1 $\rightarrow$ LUMO (39%)	349	3.55	0.000	0.003	HOMO-1 $\rightarrow$ LUMO (39%)	353	3.51	0.000	0.001	353	350	3.54	0.000	0.001	0.001
<b>1</b>	$S_0 \rightarrow S_1$	404	3.07	0.880	11.714	HOMO $\rightarrow$ LUMO (96%)	396	3.13	0.891	11.617	HOMO $\rightarrow$ LUMO (96%)	390	3.14	1.044	12.853	390	374	3.31	1.044	12.853	12.853
	$S_0 \rightarrow S_2$	355	3.49	0.000	0.003	HOMO $\rightarrow$ LUMO (95%)	353	3.51	0.000	0.000	HOMO $\rightarrow$ LUMO (95%)	389	3.07	0.000	0.000	389	355	3.49	0.000	0.000	0.000
<b>2</b>	$S_0 \rightarrow S_1$	413	3.00	0.977	13.282	HOMO $\rightarrow$ LUMO (96%)	404	3.05	1.004	13.355	HOMO $\rightarrow$ LUMO (96%)	404	3.07	1.185	14.890	404	382	3.25	1.185	14.890	14.890
	$S_0 \rightarrow S_2$	361	3.43	0.025	0.292	HOMO $\rightarrow$ LUMO (96%)	358	3.47	0.002	0.022	HOMO $\rightarrow$ LUMO (96%)	389	3.11	0.002	0.021	389	358	3.46	0.002	0.021	0.021
<b>3</b>	$S_0 \rightarrow S_1$	406	3.06	0.862	11.512	HOMO $\rightarrow$ LUMO (96%)	398	3.11	0.876	11.483	HOMO $\rightarrow$ LUMO (96%)	399	3.11	1.028	12.740	399	377	3.29	1.028	12.740	12.740
	$S_0 \rightarrow S_2$	356	3.48	0.001	0.010	HOMO $\rightarrow$ LUMO (95%)	355	3.49	0.000	0.000	HOMO $\rightarrow$ LUMO (95%)	396	3.06	0.000	0.001	396	357	3.47	0.000	0.001	0.001
<b>4</b>	$S_0 \rightarrow S_1$	424	2.93	0.910	12.694	HOMO $\rightarrow$ LUMO (96%)	406	3.05	0.966	12.928	HOMO $\rightarrow$ LUMO (96%)	405	3.06	1.157	14.662	405	385	3.22	1.157	14.662	14.662
	$S_0 \rightarrow S_2$	371	3.34	0.114	1.399	HOMO $\rightarrow$ LUMO (96%)	358	3.46	0.006	0.068	HOMO $\rightarrow$ LUMO (96%)	386	3.21	0.006	0.058	386	359	3.45	0.005	0.058	0.058
<b>5</b>	$S_0 \rightarrow S_1$	400	3.10	0.758	9.998	HOMO $\rightarrow$ LUMO (96%)	387	3.20	0.787	10.023	HOMO $\rightarrow$ LUMO (96%)	383	3.21	0.956	11.532	383	366	3.38	0.956	11.532	11.532
	$S_0 \rightarrow S_2$	356	3.49	0.001	0.008	HOMO $\rightarrow$ LUMO (96%)	350	3.54	0.000	0.000	HOMO $\rightarrow$ LUMO (96%)	383	3.21	0.000	0.001	383	351	3.53	0.000	0.001	0.001
<b>6</b>	$S_0 \rightarrow S_1$	400	3.10	0.740	9.733	HOMO $\rightarrow$ LUMO (96%)	386	3.21	0.766	9.739	HOMO $\rightarrow$ LUMO (96%)	384	3.23	0.925	11.105	384	365	3.40	0.925	11.105	11.105
	$S_0 \rightarrow S_2$	354	3.50	0.001	0.006	HOMO $\rightarrow$ LUMO (96%)	349	3.55	0.000	0.003	HOMO $\rightarrow$ LUMO (96%)	403	3.07	0.000	0.002	403	350	3.54	0.000	0.002	0.002
<b>7</b>	$S_0 \rightarrow S_1$	398	3.12	0.759	9.950	HOMO $\rightarrow$ LUMO (96%)	387	3.20	0.783	9.986	HOMO $\rightarrow$ LUMO (96%)	383	3.07	0.926	11.140	383	366	3.39	0.926	11.140	11.140
	$S_0 \rightarrow S_2$	353	3.51	0.002	0.028	HOMO $\rightarrow$ LUMO (100%)	350	3.55	0.000	0.004	HOMO $\rightarrow$ LUMO (100%)	390	2.95	0.000	0.003	390	351	3.53	0.000	0.003	0.003
<b>8</b>	$S_0 \rightarrow S_1$	418	3	0.870	11.988	HOMO $\rightarrow$ LUMO (100%)	402	3.08	0.922	12.198	HOMO $\rightarrow$ LUMO (100%)	420	2.95	1.159	15.154	420	397	3.12	1.159	15.154	15.154
	$S_0 \rightarrow S_2$	362	3.43	0.025	0.294	HOMO $\rightarrow$ LUMO (100%)	354	3.50	0.001	0.006	HOMO $\rightarrow$ LUMO (100%)	408	3.04	0.001	0.002	408	365	3.40	0.000	0.002	0.002
<b>9</b>	$S_0 \rightarrow S_1$	434	2.86	0.743	10.611	HOMO $\rightarrow$ LUMO (100%)	414	3.00	0.790	10.763	HOMO $\rightarrow$ LUMO (100%)	408	3.04	0.967	12.282	408	386	3.21	0.967	12.282	12.282
	$S_0 \rightarrow S_2$	373	3.33	0.010	0.126	HOMO $\rightarrow$ LUMO (100%)	360	3.44	0.002	0.022	HOMO $\rightarrow$ LUMO (100%)	408	3.04	0.002	0.024	408	358	3.46	0.002	0.024	0.024

in the  $S_0 \rightarrow S_1$  transition for 1–9 are shown in the ESI.† The lowest energy HOMO  $\rightarrow$  LUMO transition broadly mimics the  $\pi$ - $\pi^*$  transition as observed in TPP and the  $S_0 \rightarrow S_2$  transition in pyrene. For compound 1, a small bathochromic shift in the vertical transition wavelength is observed and is attributed to the electron-donating nature of the alkyl groups. For compound 2 and 3 (4)  $n$ - $\pi^*$  transitions involving O (S) are observed, which increases the effective conjugation resulting in bathochromic shifts in the vertical absorption with the largest effect of sulfur. However, the peripheral phenyl units in compound 2 are isolated from the chromophore. Remarkably, F is involved in the  $n$ - $\pi^*$  transition only for compound 5, *i.e.* *p*-fluorophenyl, yet not in compound 6, *i.e.* the 3,5-difluorophenyl substituent or compound 7, *i.e.* 3,5-bis(trifluoromethyl)phenyl. In all three cases, the absorption maximum remains unaltered in comparison to TPP. For compounds 1, 5, 6, and 7 a minor contribution from the HOMO–1  $\rightarrow$  LUMO+1 transition of approx. 2% is observed similar to TPP, diminished in comparison to the 10% this transition contributes in pyrene. A delocalization of electron density toward the ester functionality is observed for compound 8 and into the thienyl units for compound 9. The ground state to first excited state absorptions that include state-specific correction in THF solution are listed along with experimental data as acquired in THF. The computed values match well with the experimental data within few nm in general. For compounds 2, 7, and 8, a 0.1–0.2 eV shift is observed between the theory and the experiment, Table 3.

### Emission in the solid state

The photophysical quantum yield data in the solid state were also collected. The emission spectra of compounds 1–9 obtained in the crystalline state and thin films were acquired, Fig. 6 and 7. In general, we observed a bathochromic shift going from solution to crystalline solid-state emission by as low as 0.1 eV in the case of 1 and as high as 0.5 eV in the case of 9. In addition, a bathochromic shift was also observed in the spin-coated thin film emission *versus* the solution. It is noteworthy that the emission in the crystalline state *vs.* thin films for 9 is exceptionally different, with a  $\lambda_{\text{max}}$  around 585 nm for the crystalline powder

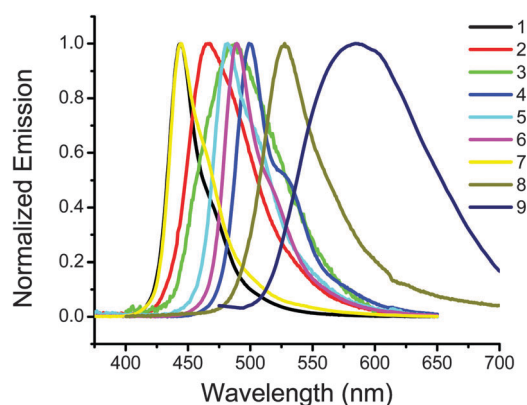


Fig. 6 Normalized fluorescence spectra of crystalline samples 1–9 at  $\lambda_{\text{ex}} = 320$  nm.

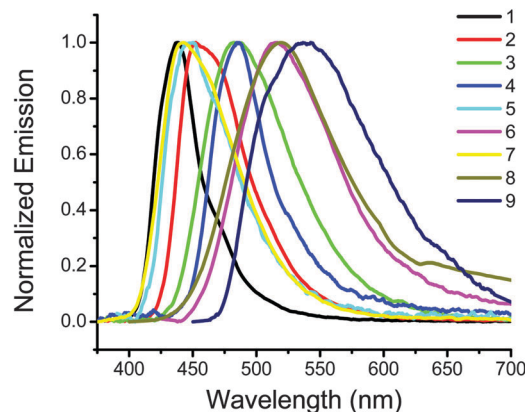


Fig. 7 Normalized fluorescence spectra of 1–9 in thin films at  $\lambda_{\text{ex}} = 320$  nm.

and 540 nm for thin films. In the case of 9, this might be due to aggregate emission in the crystalline state, which is suppressed or substantially modified in thin films. The absolute fluorescence quantum yield in the crystalline state ranged from 0.048 for compound 9 to 0.918 for compound 7, Table 4. This trend was mirrored in thin films with 0.077 for 9 and 0.911 for 7. With the exception of 1, 6, and 8, the compounds are more emissive in thin films than in the crystalline state. Noteworthy is compound 3, which shows merely 12% quantum yield in the crystalline form yet 88% in thin films. This dramatic variation is attributed to the different packing of molecules in the crystal *vs.* thin films. In most cases, an increased intermolecular interaction is observed going from solution to thin films and finally to crystalline solids. In general, thin films show a lower crystallinity than a precipitated material, especially when the evaporation of the solvent is forced rapidly by spin-coating. The amorphous phases in thin films are more susceptible to encapsulate residual solvent molecules and are therefore loosely packed. This might account for the increase in quantum yield of compounds 2, 3, 4, 5 and 9 in thin films *vs.* crystalline state. However, 1, 6, and 8 display the opposite trend and might signify an increase in packing density in thin films or it might be due to more complicated deactivation pathways. Our findings infer that the photophysical properties of these compounds are sensitive

Table 4 Absolute fluorescence quantum yield of compounds 1–9 in crystalline state (CR) and thin films (TF)  $\lambda_{\text{ex}} = 320$  nm

Compound	$\Phi_{\text{CR}}$	$\Phi_{\text{TF}}$
1	0.735	0.540
2	0.539	0.747
3	0.124	0.881
4	0.464	0.506
5	0.183	0.306
6	0.776	0.485
7	0.918	0.911
8	0.626	0.222
9	0.048	0.077

CR = crystalline state; TF = thin films prepared on glass substrates from solutions of  $5 \times 10^{-4}$  M in dichloromethane. The average error in the measurements above was 0.004.

to the level of packing in the solid-state and are consistent with previous reports of a red-shift in the emission spectra of pyrene derivatives due to different types of packing<sup>60,61</sup> as different packings lead to different polarization energies, variations in ionization potential and electron affinities and hence transition energies.<sup>62</sup> In general, for TPP, annealed thin films and crystalline solids exhibit different photoluminescence properties while attaining the same crystal form.<sup>55</sup> In addition, different packing modes of 1-acetyl-3-(4-methoxyphenyl)-5-(1-pyrenyl)-pyrazoline (AMPP) that resulted from various crystallization strategies yielded different optical properties of the same compound.<sup>60</sup>

## Electrochemistry

The ionization potential (IP) of pyrene *vs.* vacuum was determined to be 5.6 eV (0.84 V *vs.* FcCp<sub>2</sub><sup>+0</sup> in DCM).<sup>63</sup> Solution electrochemistry experiments showed that the oxidation potential of pyrene is 1.3 eV *vs.* SCE<sup>64</sup> and an effective blocking of reactive 1,3,6, and 8-positions in pyrene is necessary to observe a clear, one electron, quasi-reversible oxidation to yield a relatively stable cation radical such as in TPP.<sup>65</sup> The oxidation potential of TPP was reported as 1.13 eV *vs.* SCE.<sup>64</sup> Functionalizing the TPP with electron donating groups on the dangling phenyl groups such as in compounds 1–4 or a 1,3,6,8-tetrathienyl-substituted pyrene 9 shifts the oxidation waves to a less positive potential of ~5.4 eV, and hence decreases their IPs *vs.* vacuum, Fig. 8 and Table 5, a behavior that was observed before.<sup>63</sup> This trend is still observed for compound 5 with one electron-withdrawing fluorine atom per dangling phenyl unit. On the other hand, adding two electron-withdrawing trifluoromethyl groups per phenyl unit in 7 and one ester group per phenyl unit in 8 shifts the oxidation potential in the opposite direction, increasing the IPs *vs.* vacuum by 0.30 and 0.50 eV compared to 1–5. A similarly structured 0.4 eV increase in the electron affinity *vs.* vacuum is observed for 7 and 8 compared to the series 1–5. Compound 9 exceptionally does not follow the trend of 1–5 and exhibits a 0.1 eV increase in electron affinity *vs.* vacuum. Due to insolubility of 6, no data were acquired.

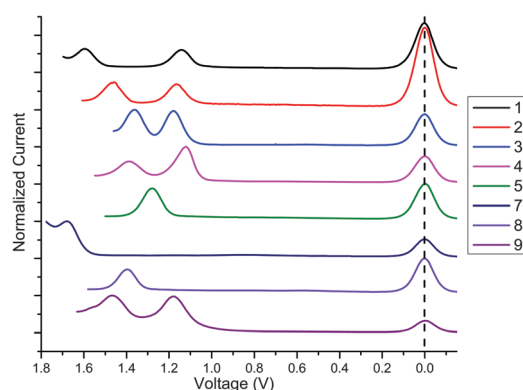


Fig. 8 Differential pulse voltammetry (DPV) on the series 1–5 and 7–9 in dichloromethane. Decamethyl-ferrocene (right) was used as an internal standard.

Table 5 Electrochemical potentials and electrochemically estimated solid-state ionization potentials

	$E_{1/2}^{+/0}$ <sup>a</sup> [V]	$E_{1/2}^{2+/+}$ <sup>a</sup> [V]	$E_{1/2}^{+/0}$ <sup>b</sup> [V]	$E_{1/2}^{2+/+}$ <sup>b</sup> [V]	IP(s) <sup>c</sup> [eV]	$\lambda_{\text{onset}}$ [nm]	$E_g^{\text{opt},f}$ [eV]	EA(s) <sup>f</sup> [eV]
1	1.14	1.7	0.6	1.16	5.4	419	2.96	2.44
2	1.16	1.46	0.62	0.92	5.4	420	2.95	2.45
3	1.18	1.36	0.64	0.82	5.4	420	2.95	2.45
4	1.12	1.39	0.58	0.85	5.4	431	2.88	2.52
5	1.28	— <sup>e</sup>	0.74	— <sup>e</sup>	5.5	409	3.03	2.47
6	— <sup>d</sup>	— <sup>d</sup>	— <sup>d</sup>	— <sup>d</sup>	— <sup>d</sup>	410	3.02	— <sup>d</sup>
7	1.68	— <sup>e</sup>	1.14	— <sup>e</sup>	5.9	408	3.04	2.86
8	1.4	— <sup>e</sup>	0.86	— <sup>e</sup>	5.7	430	2.88	2.82
9	1.18	1.47	0.64	0.95	5.4	450	2.76	2.64

<sup>a</sup> Data collected *versus* the decamethylferrocene/decamethylferrocenium (DMFc/DMFc<sup>+0</sup>) scale. <sup>b</sup> Data converted to the ferrocene/ferrocenium (Fc/Fc<sup>+</sup>) scale: (DMFc/DMFc<sup>+0</sup>) was measured to be −0.54 *vs.* FcCp<sub>2</sub><sup>+0</sup> in DCM. <sup>c</sup> Estimated according to IP(s) =  $eE_{1/2}^{+/0}$  [*vs.* Fc/Fc<sup>+</sup>] + 4.8 eV. <sup>d</sup> Data could not be recorded, since compound 6 was not soluble in DCM. <sup>e</sup> Second oxidation was not detected in the potential window scanned. <sup>f</sup> Value taken from onset of absorption in chloroform and converted using  $E = 1240/\lambda$ .

## X-ray crystal structure analysis

The X-ray crystal structures of compounds 1, 2, 4, 5, 7 and 9 were obtained and their packings were analyzed. The crystal structure of 9 was previously reported (CCDC 287258).<sup>36</sup> Only compound 1 crystallizes in the orthorhombic *Pbca* space group, while all the other compounds crystallize in the same centrosymmetric space group No. 14, which is set as *P2<sub>1</sub>/c* for 2, 4, and 9 and *P2<sub>1</sub>/n* for 5, and 7, Table 6. In all six crystals the reported molecules reside on inversion centers, thus only half a molecule is in the asymmetric unit and labeled. The substituents, which are the substituted phenyl rings in 1, 2, 4, 5, and 7 and the thienyl rings in 9, connected to C1 and C3 are in all cases not coplanar with the main pyrene core as evident in ESI† The dihedral angles between the pyrene core and the phenyl rings (thienyl rings in 9) are 53.9° and 57.3° for 1, 44.4° and 67.2° for 2, 41.7° and 53.0° for 4, 44.8° and 44.8° for 5, 53.6° and 53.8° for 7, and 54.6° and 59.4° for 9. The molecular structure of compound 9 as published before<sup>36</sup> and as synthesized in the course of the present work hardly differ; for instance, the dihedral angles between the pyrene core and the thienyl rings in 9 are equal to 56.1° and 59.5° as reported by Zhang *et al.*<sup>36</sup> and the small differences in these parameters can be related to the difference in the temperatures of experiments. There are no short intermolecular contacts between molecules responsible for specific interactions such as  $\pi$ – $\pi$  stacking interactions (see ESI†) (Fig. 9).

## OLED device data

The series of compounds was carefully selected and characterized in OLED applications. Due to their promising thin film quantum yields, compounds 2, 3, 4 as well as 7 were probed due to their electroluminescence (EL) properties, while compounds 5, 6, 8 and 9 were considered less promising and hence were excluded from the current work. Furthermore, compound 1 was previously reported in OLED application in a patent application<sup>46</sup> and a publication.<sup>47</sup> Compound 7 was included in this study despite a patent application dating back to 2006<sup>48,49</sup>

Table 6 Main crystallographic data

	1	2	4	5	7	9
Empirical formula	C <sub>56</sub> H <sub>58</sub>	C <sub>64</sub> H <sub>42</sub> O <sub>4</sub>	C <sub>44</sub> H <sub>34</sub> S <sub>4</sub>	C <sub>40</sub> H <sub>22</sub> F <sub>4</sub>	C <sub>48</sub> H <sub>18</sub> F <sub>24</sub>	C <sub>32</sub> H <sub>18</sub> S <sub>4</sub>
Formula weight	731.02	875.04	690.95	578.61	1050.64	530.70
Temperature, K	100	100	297	100	100	100
Crystal system	Orthorhombic	Monoclinic	Monoclinic	Monoclinic	Monoclinic	Monoclinic
Space group	<i>Pbca</i>	<i>P2<sub>1</sub>/c</i>	<i>P2<sub>1</sub>/c</i>	<i>P2<sub>1</sub>/n</i>	<i>P2<sub>1</sub>/n</i>	<i>P2<sub>1</sub>/c</i>
<i>a</i> , Å	14.829(6)	15.87(3)	16.4099(17)	3.914(3)	4.795(5)	13.688(3)
<i>b</i> , Å	12.324(5)	7.203(12)	6.9907(7)	11.932(10)	14.347(14)	8.4634(16)
<i>c</i> , Å	23.182(9)	19.66(3)	16.3466(17)	27.87(2)	28.88(3)	10.987(2)
$\alpha$ , °	90	90	90	90	90	90
$\beta$ , °	90	106.884(17)	114.8800(10)	90.739(12)	92.154(14)	111.999(3)
$\gamma$ , °	90	90	90	90	90	90
Volume, Å <sup>3</sup>	4236(3)	2151(6)	1701.2(3)	1301.6(18)	1985(3)	1180.2(4)
<i>Z</i>	4	2	2	2	2	2
$\rho_{\text{calc}}$ , g cm <sup>-3</sup>	1.146	1.351	1.349	1.476	1.7576	1.493
<i>F</i> (000)	1576	916	724	596	1044	548
$\mu$ , mm <sup>-1</sup>	0.064	0.083	0.312	0.104	0.181	0.425
Independent reflections	2913	1736	5209	2336	3678	5209
<i>R</i> <sub>1</sub> ; <i>wR</i> <sub>2</sub> ( <i>I</i> > 2 $\sigma$ ( <i>I</i> ))	0.0467, 0.0968	0.0552, 0.1115	0.0576, 0.1351	0.1071, 0.2833	0.0700, 0.1493	0.0335, 0.0891
GOF on <i>F</i> <sup>2</sup>	1.050	1.090	1.018	1.064	1.029	1.060

because it is highly fluorinated and exhibits a high quantum yield in thin films. Specifically, the electroluminescence (EL) properties of compounds 2, 3, 4 and 7 were investigated in a standard, single-layer ITO/PEDOT:PSS/[compounds]/Ca/Al sandwich geometry where the active layers were deposited by physical vapor deposition (PVD). The active layer thickness was 80 nm for all the investigated devices. Fig. 10a depicts the current density–voltage–luminescence (*J*–*V*–*L*) characteristics of devices with 2, 3, and 4 serving as the emissive layers. For the sake of better readability, the corresponding *J*–*V*–*L* characteristics of 7 are included in the ESI.† All relevant device parameters (turn-on voltage, maximum luminance, and luminance efficiency) are listed in Table 7. Peak luminescence values of 85 cd m<sup>-2</sup> at 6 V, 13 542 cd m<sup>-2</sup> at 8.2 V, and 6 902 cd m<sup>-2</sup> at 8 V were recorded for devices based on 4, 2 and 3, respectively. Low onset voltages of 2.9, 2.8, and 2.9 V were observed for 4, 2, and 3, respectively. These values are close to the optical gap of approximately 2.6 eV of the investigated tetraryl pyrenes, which is indicative of efficient injection of charge carriers in all devices. Peak luminance efficiencies were 0.005 cd A<sup>-1</sup> (4.6 V), 2 cd A<sup>-1</sup> (3.6 V) and 2.6 cd A<sup>-1</sup> (4.8 V) for 4, 2 and 3, respectively. These performance figures, with the exception of 4, are rather impressive considering that these results were obtained from simple, not optimized single-layer geometries.

Remarkably, devices based on 4 show approximately the same current density as the other devices; however, the peak brightness and luminance are more than two orders of magnitude lower in comparison to the other two investigated tetraryl pyrenes. This observation is consistent with the presence of a charge carrier imbalance.

Interestingly, the trend of remarkably low onset voltages did not continue for the (trifluoromethyl)phenyl-decorated compound 7, which turned-on at a rather high bias voltage of 9.0 V. In addition, a peak luminance of 7 cd m<sup>-2</sup> was attained at a quite high voltage of 12 V. Considering that 7 exhibited a PLQY close to unity in thin films, these findings indicate the presence of a severe charge carrier injection- and/or transport issue.

While the CV data put the ionization potential of 7 at a deeper –5.9 eV compared to –5.4 eV of 2, 3 and 4, it is still noteworthy that the transition from the injection-limited conduction (ILC) – to the space-charge-limited current (SCLC)-regime is observable already at 3.9 V, which is less than half the onset voltage. A previous work on fluorinated fluorescent compounds by Lee *et al.*<sup>66</sup> also showed a significantly higher turn-on voltage for highly fluorinated compounds which was explained by the formation of transport-affecting charge traps by the electron-withdrawing fluorinated functionalities.<sup>67</sup> In addition, it is possible that, similar to the observations made by Giebler *et al.*,<sup>68</sup> these bulk traps cause the buildup of an injection prohibiting counter field (similar to the MEMOLED concept reported by Asadi *et al.*<sup>69</sup> where this field is generated by a ferroelectric).

The EL properties and their time-evolution were observed over a period of 300 s of continuous operation and fixed current densities (see Fig. 10b). Devices based on 4, 2 and 3 featured a sky-blue emission color with a broad molecular emission peaking at 470, 471 and 479 nm, respectively, while 7 is characterized by a structure-less blue EL with a peak at 456 nm. Emission spectra of 3 were structure-less, while the presence of a minor shoulder at 484 nm was detectable in the corresponding EL spectra of 4. Regarding 2, the appearance of a small emission peak at 593 nm, likely attributable to phosphorescence emission,<sup>70–72</sup> as well as the existence of a distinct shoulder at 450 nm is notable. From the thin-film PL spectra (see Fig. 7) of 2 it is clear that the presence of microcavity effects<sup>73</sup> in the device led to an attenuation of the emission maximum at 450 nm and a boost of the small emission shoulder at 470 nm found in PL effectively exchanging the emission maximum and the shoulder position in the corresponding EL spectra.

Owing to the additional high-energy contributions in the EL spectra of 7 and 2, the Commission Internationale de l'Éclairage 1931 (CIE1931) (*x*, *y*) coordinates after power-on of 7 and 2 are (0.153, 0.124) and (0.163, 0.200), hence noticeably more blue than 4 and 3 based devices with (0.148, 0.244) and (0.148, 0.243). As can be inferred from the time evolution of the EL spectra

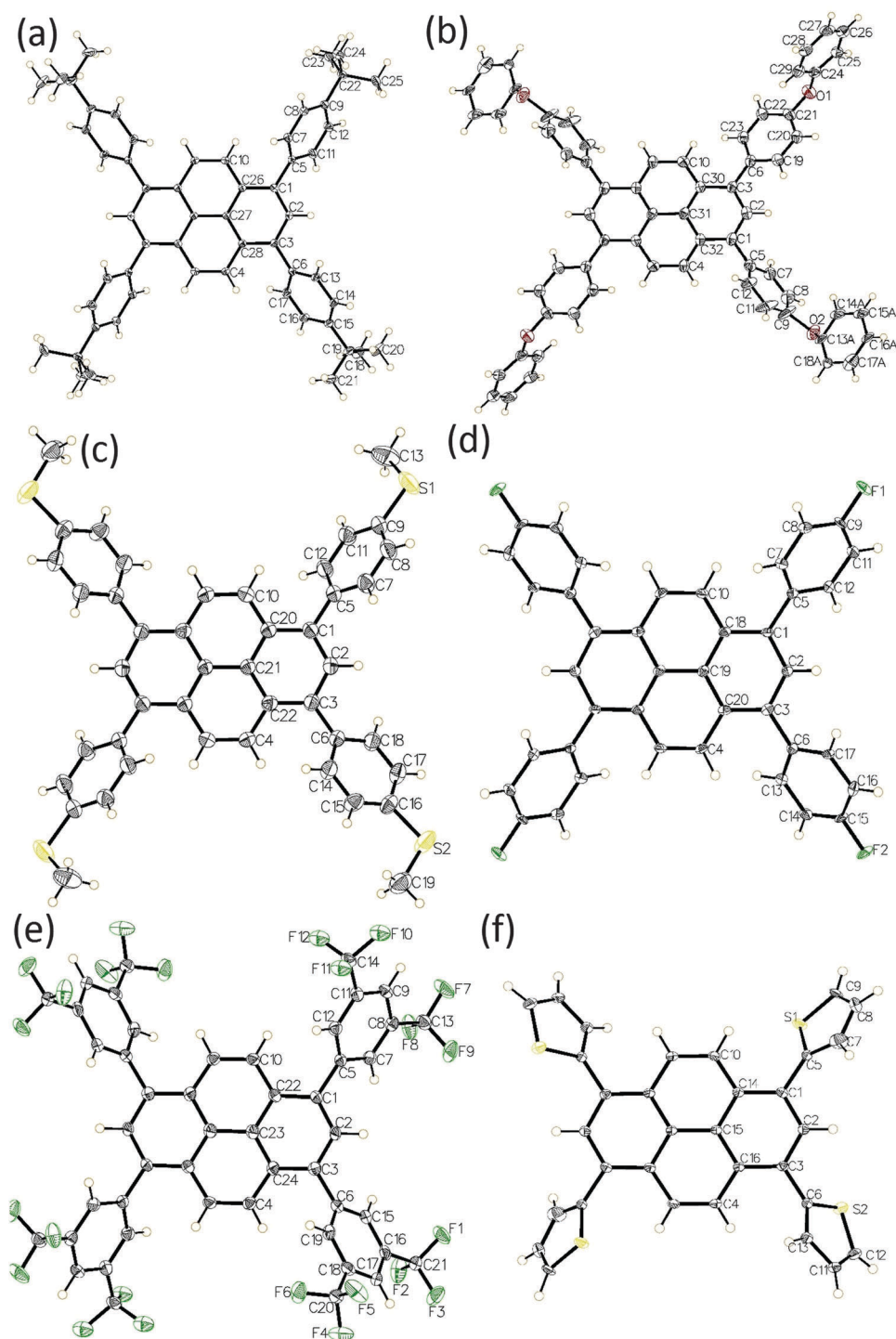


Fig. 9 The molecular structures of compounds (a) **1**, (b) **2**, (c) **4**, (d) **5**, (e) **7**, and (f) **9**, showing the atomic numbering and 50% probability displacement ellipsoids.

depicted in Fig. 10b, no signs of material degradation are spectrally visible for **2** and **3**, while hints of a degradation process are observable in the EL spectra of **4** by the formation of two shoulders at 555 nm and 593 nm after continuous operation of 300 s. Similarly, signs of material degradation are present in **7** where the emergence of a low energy emission with a small peak at 620 nm and the formation of distinct

shoulders at 508 nm are evident. It is noted that all devices are free of any signs of excimer emission usually observable for unsubstituted pyrene.<sup>74</sup>

Overall, the presented tetraryl pyrenes already demonstrate impressive performance figures with respect to the obtained brightness and current efficiency values in non-optimized single-layer device architectures. Even more impressive are the observed

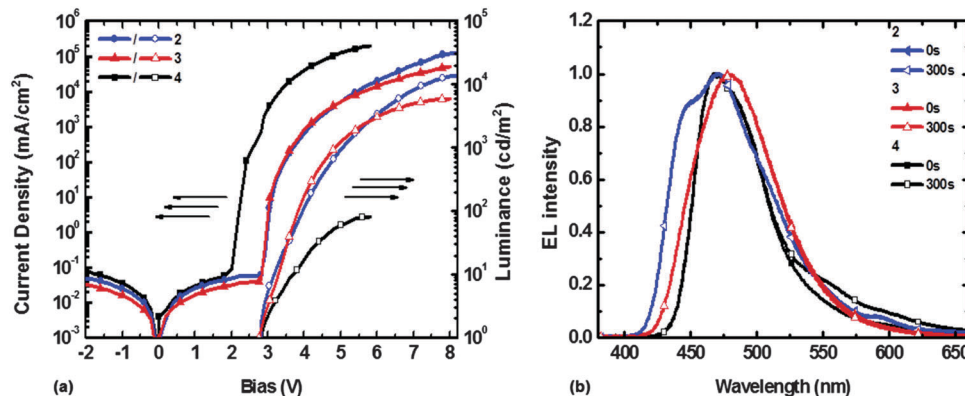


Fig. 10 (a) Current density (filled symbols) and luminance (open symbols) as a function of the bias voltage of ITO/PEDOT:PSS/2, 3, 4/Ca/Al devices and (b) the time-dependent evolution of the EL emission profile over the course of 5 minutes of continuous operation of 2, 3 and 4 at applied current densities of  $10^3$ ,  $5 \times 10^2$  and  $4 \times 10^4$  mA cm $^{-2}$ , respectively.

Table 7 Electroluminescent characteristics of the investigated compounds in a single-layer geometry

Compound	$V_{on}^a$ [V]	$L_{max}$ [cd m $^{-2}$ ]	$H^b$ [cd A $^{-1}$ ]	CIE1931 [x, y]
2	2.8	13 542	2.0000	0.163, 0.200
3	2.9	6902	2.6000	0.243
4	2.9	85	0.0050	0.148, 0.244
7	8.6	7	0.0039	0.153, 0.124

<sup>a</sup> Voltage at a luminance of 1 cd m $^{-2}$ . <sup>b</sup> Value of the maximum efficiency.

turn-on voltages being as low as 2.8 V in a single-layer architecture, which are among the lowest for blue-emitting OLEDs.<sup>75</sup> In addition, the obtained performance values compare favorably to blue electrofluorescent devices with equally simple device architectures and active layers based on dendronized or polymerized pyrene derivatives.<sup>76–79</sup> Furthermore, by taking the human eye response curve into consideration, it has to be noted that the presented OLED devices are able to outperform the previously mentioned 1,3,6,8-tetrakis[4-2,2-diphenylvinyl]-phenyl]pyrene multilayer devices based on the estimate that the human eye has 1/10th the sensitivity at  $\sim 470$  nm as at 545 nm.

It is expected that device efficiencies can be further improved by introduction of appropriate charge transport- and injection layers in order to ensure a more balanced charge injection and transport.<sup>80</sup>

For contrast, 13 000 cd m $^{-2}$  and *ca.* 2 cd A $^{-1}$  in a single layer device which in the absence of any hole or electron transport layer (HTL or ETL) can be compared to one of the best blue light-emitting polymer devices, recently published,<sup>81</sup> which reached *ca.* 1 cd A $^{-1}$  in the single layer device configuration and 9.7 cd A $^{-1}$  in the optimised heterojunction device geometry. Table 8 includes an overview over recent literature reports on OLEDs. It is important to note that all of these examples include at least an electron transport layer in the device stack, whereas the performance data of our devices are comparable.

## Conclusions

The series of nine 1,3,6,8-tetraarylpyrenes exhibit positive solvatochromic behavior. DFT calculations verify the  $S_0 \rightarrow S_1$  transition to be HOMO–LUMO character as observed for 1,3,6,8-tetraphenylpyrene

Table 8 Overview of recent OLED performance with a simple device geometry

Stack	CIE	LE [cd A $^{-1}$ ]	EM peak [nm]	$V_{on}$ [V]	$L_{max}$ [cd m $^{-2}$ ]	Material	Ref.
ITO/PEDOT:PSS/EML/TPBi/LiF/Al	(0.15, 0.09)	2.48	448	3.3	7300	2P-TCTA–5P-TCTA	82
ITO/PEDOT:PSS (30 nm)/EML (20 nm)/TPBi (35 nm)/Ca (10 nm):Ag (100 nm)	(0.16, 0.10)	1.46	444	4.9	3983	CAC	83
	(0.22, 0.22)	0.10	448	5.8	400	BAB	
	(0.18, 0.16)	0.60	448	5.5	2945	BAC	
ITO/MoO $_3$ (10 nm)/NPB(60 nm)/EML (30 nm)/TPBi (30 nm)/LiF (1 nm)/Al	(0.15, 0.11)	0.34	451	3.7	922	mTPA–CN–mTPA	84
ITO/NPB (70 nm)/TCTA (10 nm)/PhPC (30 nm)/TPBi (30 nm)/LiF (1 nm)/A	(0.15, 0.05)	1.8	420	3.8	2267	PhPC	85
ITO/CFx/PhN-OF(2)-TAZ (70 nm)/LiF/Al	(0.17, 0.24)	1.8	476	3.5	367	PhN-OF(2)-TAZ	86

ITO: indium tin oxide; PEDOT:PSS: poly(3,4-ethylenedioxythiophene):poly(styrenesulfonate); EML: emissive layer; TPBi: 1,3,5-tris(1-phenylbenzimidazol-2-yl)-benzene; LiF: lithium fluoride; Al: aluminum; 2P-TCTA 4,4',4''-tris(carbazol-9-yl)-triphenylamine spaced by 2 phenyl units between two N atoms; 5P-TCTA: 4,4',4''-tris(carbazol-9-yl)-triphenylamine spaced by 5 phenyl units between two N atoms; Ca: calcium; Ag: silver; CAC: 9,10-bis(30,50-bis(1-phenyl-1H-benzo[d]imidazol-2-yl)biphenyl-4-yl)-anthracene; BAB: 9,10-bis(3,6-bis(3,6-di-*tert*-butyl-carbazol-9-yl)-carbazole)biphenyl-4-yl-anthracene; BAC: 9-[4-(3,6-bis(3,6-di-*tert*-butyl-carbazol-9-yl)-carbazole)-phenyl]-10-[4-(30,50-bis(1-phenyl-1H-benzo[d]imidazol-2-yl)-phenyl)-anthracene; MoO $_3$ : molybdenum trioxide; NPB: *N,N*-di(1-naphthyl)-*N,N*-diphenyl-(1,1-biphenyl)-4,4-diamine; TCTA: 4,4,4-tris(*N*-carbazolyl)triphenylamine; PhPC: 9-(4-(10-phenylanthracene-9-yl)phenyl)-9H-carbazole; CFx: carbon monofluoride; PhN-OF(2)-TAZ: 9,9,9',9'-tetrabutyl-7'-(4-(5-(4-(*tert*-butyl)phenyl)-4-phenyl-4H-1,2,4-triazol-3-yl)phenyl)-*N,N*-diphenyl-9H,9'H-[2,2'-bifluoren]-7-amine.

and in contrast to pyrene. The fluorescence quantum yield in solution ranged from 0.76 (6) to 0.98 (2), while the quantum yield peaked for compound 7 in the solid state at 0.91. The absence of short-contacts and interactions in the solid state was verified by X-ray crystallography. Compounds 2, 3, 4, and 7 were tested in OLEDs in an unoptimized single-layer device geometry. Efficient injection of charge carriers was observed for all devices along with blue electroluminescence with low turn-on voltages and high maximum luminances.

## Acknowledgements

This work was supported by the Petroleum Research Fund (PRF) of the American Chemical Society (grant #: 47343-B10). The authors are grateful to this support. B.R.K. and B.W. acknowledge the Arab Fund Scholarship Program for financial support. The authors thank Dr. Veaceslav Coropceanu, Mr. Alexandr Fonari and Mr. Stephen B. Shirring for fruitful discussions. M.A. gratefully acknowledges the financial support of the Klima- und Energiefonds Project PLASMOLED 3726090. TVT and RC were supported by NSF PREM grants DMR-0934212 and DMR-1523611.

## References

- 1 Y. Chen, Q. Lv, Z. Q. Liu and Q. Fang, *Inorg. Chem. Commun.*, 2015, **52**, 38–40.
- 2 A. Singh, R. Singh, M. Shellaiah, E. C. Prakash, H. C. Chang, P. Raghunath, M. C. Lin and H. C. Lin, *Sens. Actuators, B*, 2015, **207**, 338–345.
- 3 R. W. Sinkeldam, N. J. Greco and Y. Tor, *Chem. Rev.*, 2010, **110**, 2579–2619.
- 4 T. M. Figueira-Duarte and K. Müllen, *Chem. Rev.*, 2011, **111**, 7260–7314.
- 5 V. Balzani, P. Ceroni and A. Juris, *Photochemistry and Photophysics: Concepts, Research, Applications*, Wiley, 2014.
- 6 B. Valeur and M. N. Berberan-Santos, *Molecular Fluorescence: Principles and Applications*, John Wiley & Sons, 2013.
- 7 J. B. Birks, *Photophysics of Aromatic Molecules*, 1970.
- 8 I. B. Berlman, *Handbook of Fluorescence Spectra of Aromatic Molecules*, Academic Press, New York, 1971.
- 9 C. A. Parker and C. G. Hatchard, *Trans. Faraday Soc.*, 1963, **59**, 284–295.
- 10 G. K. Bains, S. H. Kim, E. J. Sorin and V. Narayanaswami, *Biochemistry*, 2012, **51**, 6207–6219.
- 11 M. Shimizu and T. Hiyama, *Chem. – Asian J.*, 2010, **5**, 1516–1531.
- 12 J. M. Casas-Solvas, J. D. Howgego and A. P. Davis, *Org. Biomol. Chem.*, 2014, **12**, 212–232.
- 13 H. Maeda, T. Maeda, K. Mizuno, K. Fujimoto, H. Shimizu and M. Inouye, *Chem. – Eur. J.*, 2006, **12**, 824–831.
- 14 C. H. Yang, T. F. Guo and I. W. Sun, *J. Lumin.*, 2007, **124**, 93.
- 15 T. M. Figueira-Duarte, S. C. Simon, M. Wagner, S. I. Druzhinin, K. A. Zachariasse and K. Müllen, *Angew. Chem., Int. Ed.*, 2008, **47**, 10175–10178.
- 16 J. A. Mikroyannidis, *Synth. Met.*, 2005, **155**, 125–129.
- 17 J. Grimshaw and J. Trocha-Grimshaw, *J. Chem. Soc., Perkin Trans. 1*, 1972, 1622–1623.
- 18 A. a. O. El-Ballouli, R. S. Khnayzer, J. C. Khalife, A. Fonari, K. M. Hallal, T. V. Timofeeva, D. Patra, F. N. Castellano, B. Wex and B. R. Kaafarani, *J. Photochem. Photobiol., A*, 2013, **272**, 49–57.
- 19 A. G. Crawford, A. D. Dwyer, Z. Liu, A. Steffen, A. Beeby, L.-O. Palsson, D. J. Tozer and T. B. Marder, *J. Am. Chem. Soc.*, 2011, **133**, 13349–13362.
- 20 B. R. Kaafarani, A. a. O. El-Ballouli, R. Trattng, A. Fonari, S. Sax, B. Wex, C. Risko, R. S. Khnayzer, S. Barlow, D. Patra, T. V. Timofeeva, E. J. W. List, J.-L. Brédas and S. R. Marder, *J. Mater. Chem. C*, 2013, **1**, 1638–1650.
- 21 X. Feng, J.-Y. Hu, L. Yi, N. Seto, Z. Tao, C. Redshaw, M. R. J. Elsegood and T. Yamato, *Chem. – Asian J.*, 2012, **7**, 2854–2863.
- 22 X. Feng, J. Y. Hu, F. Iwanaga, N. Seto, C. Redshaw, M. R. Elsegood and T. Yamato, *Org. Lett.*, 2013, **15**, 1318–1321.
- 23 T. Makowski, R. M. Moustafa, P. Uznanski, W. Zajaczkowski, W. Pisula, A. Tracz and B. R. Kaafarani, *J. Phys. Chem. C*, 2014, **118**, 18736–18745.
- 24 S. Chen, F. S. Raad, M. Ahmida, B. R. Kaafarani and S. H. Eichhorn, *Org. Lett.*, 2013, **15**, 558–561.
- 25 J. N. Moorthy, P. Natarajan, P. Venkatakrishnan, D.-F. Huang and T. J. Chow, *Org. Lett.*, 2007, **9**, 5215–5218.
- 26 J.-Y. Hu, X. Feng, H. Tomiyasu, N. Seto, U. Rayhan, M. R. J. Elsegood, C. Redshaw and T. Yamato, *J. Mol. Struct.*, 2013, **1047**, 194–203.
- 27 P. Anant, N. T. Lucas, J. M. Ball, T. D. Anthopoulos and J. Jacob, *Synth. Met.*, 2010, **160**, 1987–1993.
- 28 T. Oyamada, H. Uchiuzou, S. Akiyama, Y. Oku, N. Shimoji, K. Matsushige, H. Sasabe and C. Adachi, *J. Appl. Phys.*, 2005, **98**, 074506.
- 29 Z.-Q. Liang, Z.-Z. Chu, D.-C. Zou, X.-M. Wang and X.-T. Tao, *Org. Electron.*, 2012, **13**, 2898–2904.
- 30 K. C. Stylianou, R. Heck, S. Y. Chong, J. Bacsá, J. T. A. Jones, Y. Z. Khimiyak, D. Bradshaw and M. J. Rosseinsky, *J. Am. Chem. Soc.*, 2010, **132**, 4119–4130.
- 31 D. R. Coulson, *Inorg. Synth.*, 1990, **28**, 107–109.
- 32 G. Huang, Y.-Q. Sun, Z. Xu, M. Zeller and A. D. Hunter, *Dalton Trans.*, 2009, 5083–5093.
- 33 V. de Halleux, J. P. Calbert, P. Brocogens, J. Cornil, J. P. Declercq, J. L. Brédas and Y. Geerts, *Adv. Funct. Mater.*, 2004, **14**, 649–659.
- 34 C. S. Callam and T. L. Lowary, *J. Chem. Educ.*, 2001, **78**, 947–948.
- 35 Y. Sagara, T. Mutai, I. Yoshikawa and K. Araki, *J. Am. Chem. Soc.*, 2007, **129**, 1520–1521.
- 36 H. J. Zhang, Y. Wang, K. Z. Shao, Y. Q. Liu, S. Y. Chen, W. F. Qiu, X. B. Sun, T. Qi, Y. Q. Ma, G. Yu, Z. M. Su and D. B. Zhu, *Chem. Commun.*, 2006, 755–757.
- 37 J. D. Chai and M. Head-Gordon, *J. Chem. Phys.*, 2008, **128**, 084106.
- 38 S. Refaely-Abramson, R. Baer and L. Kronik, *Phys. Rev. B: Condens. Matter Mater. Phys.*, 2011, **84**, 075144.

- 39 M. J. Frisch, G. W. Trucks, H. B. Schlegel, G. E. Scuseria, M. A. Robb, J. R. Cheeseman, G. Scalmani, V. Barone, B. Mennucci, G. A. Petersson, H. Nakatsuji, M. Caricato, X. Li, H. P. Hratchian, A. F. Izmaylov, J. Bloino, G. Zheng, J. L. Sonnenberg, M. Hada, M. Ehara, K. Toyota, R. Fukuda, J. Hasegawa, M. Ishida, T. Nakajima, Y. Honda, O. Kitao, H. Nakai, T. Vreven, J. A. Montgomery, Jr., J. E. Peralta, F. Ogliaro, M. Bearpark, J. J. Heyd, E. Brothers, K. N. Kudin, V. N. Staroverov, R. Kobayashi, J. Normand, K. Raghavachari, A. Rendell, J. C. Burant, S. S. Iyengar, J. Tomasi, M. Cossi, N. Rega, J. M. Millam, M. Klene, J. E. Knox, J. B. Cross, V. Bakken, C. Adamo, J. Jaramillo, R. Gomperts, R. E. Stratmann, O. Yazyev, A. J. Austin, R. Cammi, C. Pomelli, J. W. Ochterski, R. L. Martin, K. Morokuma, V. G. Zakrzewski, G. A. Voth, P. Salvador, J. J. Dannenberg, S. Dapprich, A. D. Daniels, Ö. Farkas, J. B. Foresman, J. V. Ortiz, J. Cioslowski and D. J. Fox, *Gaussian 09, Revision D.01*, Gaussian, Inc., Wallingford CT, 2009.
- 40 R. J. Lakowicz, *Principles of Fluorescence Spectroscopy*, Plenum Press, New York, 1983.
- 41 *SAINTPlus*, Bruker AXS, Madison, WI, v. 6.2 edn., 2001.
- 42 G. M. Sheldrick, Bruker AXS, Madison, WI, V.2.0.3, Bruker/Siemens area detector absorption correction program edn., 2003.
- 43 O. V. Dolomanov, L. J. Bourhis, R. J. Gildea, J. A. K. Howard and H. Puschmann, *J. Appl. Crystallogr.*, 2009, **42**, 339–341.
- 44 T. Korzdörfer, J. S. Sears, C. Sutton and J. L. Brédas, *J. Chem. Phys.*, 2011, **135**, 204107.
- 45 M. Sase, S. Yamaguchi, Y. Sagara, I. Yoshikawa, T. Mutai and K. Araki, *J. Mater. Chem.*, 2011, **21**, 8347–8354.
- 46 J.-K. Bin, S.-W. Cha, S.-J. Lee, I.-B. Song, J.-K. Kim, D.-H. Kim, C.-G. Park and N.-S. Cho, *US Pat.*, application 20100164374A1, 2010.
- 47 W. Sotoyama, H. Sato, M. Kinoshita, T. Takahashi, A. Matsuura, J. Kodama, N. Sawatari and H. Inoue, *Dig. Tech. Pap. - Soc. Inf. Disp. Int. Symp.*, 2003, **34**, 1294–1297.
- 48 S. Akiyama, *Jpn. Kokai Tokkyo Koho Japanese Patent*, 2009004351 A 20090108, 2009.
- 49 T. Oyamada, H. Uchiuzou, C. Adachi, S. Akiyama and T. Takahashi, *PCT Int. Appl.*, WO 2006057326 A1 20060601, 2006.
- 50 Across various reports in literature, the numbering of pyrene is inconsistent. Herein we strictly follow the numbering of pyrene according to IUPAC nomenclature.
- 51 O. K. Bazyl, G. V. Maier, T. N. Kopylova and V. I. Danilova, *Zh. Prikl. Spektrosk.*, 1982, **37**, 80–86.
- 52 I. B. Berlman, *J. Phys. Chem.*, 1970, **74**, 3085–3093.
- 53 N. Nijegorodov, V. Zvolinsky and P. V. C. Luhanga, *J. Photochem. Photobiol., A*, 2008, **196**, 219–226.
- 54 K. R. Idzik, T. Licha, V. Lukes, P. Rapta, J. Frydel, M. Schaffer, E. Tauscher, R. Beckert and L. Dunsch, *J. Fluoresc.*, 2014, **24**, 153–160.
- 55 T. Oyamada, S. Akiyama, M. Yahiro, M. Saigou, M. Shiro, H. Sasabe and C. Adachi, *Chem. Phys. Lett.*, 2006, **421**, 295–299.
- 56 J. T. Henssler, X. N. Zhang and A. J. Matzger, *J. Org. Chem.*, 2009, **74**, 9112–9119.
- 57 M. Parac and S. Grimme, *Chem. Phys.*, 2003, **292**, 11–21.
- 58 M. Dierksen and S. Grimme, *J. Chem. Phys.*, 2004, **120**, 3544–3554.
- 59 U. Salzner and A. Aydin, *J. Chem. Theory Comput.*, 2011, **7**, 2568–2583.
- 60 Q. Feng, M. Wang, B. Dong, C. Xu, J. Zhao and H. Zhang, *CrystEngComm*, 2013, **15**, 3623–3629.
- 61 A. T. Haedler, H. Misslitz, C. Buehlmeier, R. Q. Albuquerque, A. Köhler and H.-W. Schmidt, *ChemPhysChem*, 2013, **14**, 1818–1829.
- 62 S. M. Ryno, C. Risko and J. L. Brédas, *J. Am. Chem. Soc.*, 2014, **136**, 6421–6427.
- 63 M. Gingras, V. Placide, J. M. Raimundo, G. Bergamini, P. Ceroni and V. Balzani, *Chem. – Eur. J.*, 2008, **14**, 10357–10363.
- 64 J. Phelps, K. S. V. Santhanam and A. J. Bard, *J. Am. Chem. Soc.*, 1967, **89**, 1752–1753.
- 65 L. S. Marcoux, J. M. Fritsch and R. N. Adams, *J. Am. Chem. Soc.*, 1967, **89**, 5766–5769.
- 66 J. K. Lee, H. H. Fong, A. A. Zakhidov, G. E. McCluskey, P. G. Taylor, M. Santiago-Berrios, H. D. Abruna, A. B. Holmes, G. G. Malliaras and C. K. Ober, *Macromolecules*, 2010, **43**, 1195–1198.
- 67 L. J. Alvey, R. Meier, T. Soos, P. Bernatis and J. A. Gladysz, *Eur. J. Inorg. Chem.*, 2000, 1975–1983.
- 68 C. Giebeler, S. A. Whitelegg, A. J. Campbell, M. Liess, S. J. Martin, P. A. Lane, D. D. C. Bradley, G. Webster and P. L. Burn, *Appl. Phys. Lett.*, 1999, **74**, 3714–3716.
- 69 K. Asadi, P. W. M. Blom and D. M. de Leeuw, *Adv. Mater.*, 2011, **23**, 865–868.
- 70 L. Qian, D. Bera and P. H. Holloway, *Appl. Phys. Lett.*, 2007, **90**, 153120.
- 71 M. A. Omary, R. M. Kassab, M. R. Haneline, O. Elbjairami and F. P. Gabbai, *Inorg. Chem.*, 2003, **42**, 2176–2178.
- 72 J. M. Lupton, A. Pogantsch, T. Piok, E. J. W. List, S. Patil and U. Scherf, *Phys. Rev. Lett.*, 2002, **89**, 167401.
- 73 V. Bulovic, V. B. Khalfin, G. Gu, P. E. Burrows, D. Z. Garbuzov and S. R. Forrest, *Phys. Rev. B: Condens. Matter Mater. Phys.*, 1998, **58**, 3730–3740.
- 74 S. M. Langenegger and R. Haner, *Chem. Commun.*, 2004, 2792–2793.
- 75 P. Kotchpradist, N. Prachumrak, R. Tarsang, S. Jungsuttiwong, T. Keawin, T. Sudyoasuk and V. Promarak, *J. Mater. Chem. C*, 2013, **1**, 4916–4924.
- 76 T. M. Figueira-Duarte, P. G. Del Rosso, R. Trattnig, S. Sax, E. J. W. List and K. Müllen, *Adv. Mater.*, 2010, **22**, 990–993.
- 77 C. J. Ou, Z. F. Lei, M. L. Sun, L. H. Xie, Y. Qian, X. W. Zhang and W. Huang, *Synth. Met.*, 2015, **200**, 135–142.
- 78 G. Zhang, M. Baumgarten, M. Auer, R. Trattnig, E. J. W. List-Kratochvil and K. Müllen, *Macromol. Rapid Commun.*, 2014, **35**, 1931–1936.
- 79 T. S. Qin, W. Wiedemair, S. Nau, R. Trattnig, S. Sax, S. Winkler, A. Vollmer, N. Koch, M. Baumgarten, E. J. W. List and K. Müllen, *J. Am. Chem. Soc.*, 2011, **133**, 1301–1303.
- 80 R. Trattnig, L. Pevzner, M. Jager, R. Schlesinger, M. V. Nardi, G. Ligorio, C. Christodoulou, N. Koch, M. Baumgarten, K. Müllen and E. J. W. List, *Adv. Funct. Mater.*, 2013, **23**, 4897–4905.

- 81 S. Nau, N. Schulte, S. Winkler, J. Frisch, A. Vollmer, N. Koch, S. Sax and E. J. W. List, *Adv. Mater.*, 2013, **25**, 4420–4424.
- 82 M. Q. Yu, S. M. Wang, S. Y. Shao, J. Q. Ding, L. X. Wang, X. B. Jing and F. S. Wang, *J. Mater. Chem. C*, 2015, **3**, 861–869.
- 83 Z. H. Zhang, W. Jiang, X. X. Ban, M. Yang, S. H. Ye, B. Huang and Y. M. Sun, *RSC Adv.*, 2015, **5**, 29708–29717.
- 84 X. J. Zhan, N. Sun, Z. B. Wu, J. Tu, L. Yuan, X. Tang, Y. J. Xie, Q. Peng, Y. Q. Dong, Q. Q. Li, D. G. Ma and Z. Li, *Chem. Mater.*, 2015, **27**, 1847–1854.
- 85 Y. Huang, X. Y. Du, S. L. Tao, X. X. Yang, C. J. Zheng, X. H. Zhang and C. S. Lee, *Synth. Met.*, 2015, **203**, 49–53.
- 86 X. J. Feng, S. F. Chen, Y. Ni, M. S. Wong, M. M. K. Lam, K. W. Cheah and G. Q. Lai, *Org. Electron.*, 2014, **15**, 57–64.